Lee J. Arnold, Martina Demuro, Nigel A. Spooner, Gavin J. Prideaux, Matthew C. McDowell, Aaron B. Camens, Elizabeth H. Reed, Josep María Parés, Juan Luis Arsuaga, José María Bermúdez de Castro, Eudald Carbonell

Single-grain TT-OSL bleaching characteristics: insights from modern analogues and OSL dating comparisons

Quaternary Geochronology, 2019; 49:45-51

Final publication at http://dx.doi.org/10.1016/j.quageo.2018.01.004

Single-grain TT-OSL bleaching characteristics: Insights from modern analogues and OSL dating comparisons

Lee J. Arnold [1]*, Martina Demuro [1], Nigel A. Spooner [2], Gavin J. Prideaux [3], Matthew C. McDowell [3], Aaron B. Camens [3], Elizabeth H. Reed [4], Josep María Parés [5], Juan Luis Arsuaga [6,7], José María Bermúdez de Castro [5], Eudald Carbonell [8].

[1] School of Earth and Environmental Sciences, Institute for Photonics and Advanced Sensing (IPAS), and Environment Institute, University of Adelaide, North Terrace Campus, Adelaide SA 5005, Australia.

[2] Defence Science and Technology Group, Third Avenue, Edinburgh, SA, 5111, Australia.

[3] College of Science and Engineering, Flinders University of South Australia, Bedford Park, SA 5042, Australia

[4] School of Earth and Environmental Sciences, and Environment Institute, University of Adelaide, North Terrace Campus, Adelaide SA 5005, Australia.

[5] Centro Nacional de Investigación sobre la Evolución Humana, CENIEH, Paseo Sierra de Atapuerca 3, 09002 Burgos, Spain.

[6] Centro Mixto Universidad Complutense e Instituto de Salud Carlos III de Evolución y Comportamiento Humanos, Monforte de Lemos 3-5, Pabellón 14, 28029 Madrid, Spain.

[7] Departamento de Paleontología, Facultad de Ciencias Geológicas, Universidad Complutense de Madrid, 28040 Madrid, Spain.

[8] Institut de Paleoecologia Humana i Evolució Social, Área de Prehistória, U. Rovira i Virgili, Plaça Imperial Tarraco 1, E-43005 Tarragona, Spain

* Corresponding author. E-mail address: lee.arnold@adelaide.edu.au

Keywords

Luminescence dating; thermally transferred optically stimulated luminescence (TT-OSL); single-grain; modern analogues; Spain; Australia.

Abstract

Previous assessments of thermally transferred optically stimulated luminescence (TT-OSL) signal resetting in natural sedimentary settings have been based on relatively limited numbers of observations, and have been conducted primarily at the multi-grain scale of equivalent dose (D_e) analysis. In this study, we undertake a series of single-grain TT-OSL bleaching assessments on nineteen modern and geological dating samples from different sedimentary environments. Daylight bleaching experiments performed over several weeks confirm that single-grain TT-OSL signals are optically reset at relatively slow, and potentially variable, rates. Single-grain TT-OSL residual doses range between 0 and 24 Gy for thirteen modern samples, with >50% of these samples yielding weighted mean D_e values of 0 Gy at 2σ. Single-grain OSL and TT-OSL dating comparisons performed on well-bleached and heterogeneously bleached late Pleistocene samples from Kangaroo Island, South Australia, yield consistent replicate age estimates. Our results reveal that (i) single-grain TT-OSL residuals can potentially be reduced down to insignificant levels when compared with the natural dose range of interest for most TT-OSL dating applications; (ii) the slow bleaching properties of TT-OSL signals may not necessarily limit their dating applicability to certain depositional environments; and (iii) non-trivial differences may be observed between single-grain and multi-grain TT-OSL bleaching residuals in some modern samples. Collectively, these findings suggest that single-grain TT-OSL dating may offer advantages over multi-grain TT-OSL dating in certain complex depositional environments.

1. Introduction

The favourable dose saturation properties of thermally transferred optically stimulated luminescence (TT-OSL) signals offer potential for establishing extended-range luminescence chronologies that exceed the traditional upper age limits of quartz OSL dating (e.g., Wang et al., 2006; Duller and Wintle, 2012; Arnold et al., 2015). However, TT-OSL signals have been shown to be optically reset at a considerably slower rate than conventional OSL signals (e.g., Duval et al 2017), meaning there is greater potential for insufficient signal resetting and associated TT-OSL age overestimation in any dating study. TT-OSL bleaching characteristics have been assessed using several approaches in the recent literature. Daylight bleaching experiments performed on a small number of samples have shown that several weeks or months of natural sunlight exposure are typically required to deplete TT-OSL signals to within 10% of background (e.g., Jacobs et al., 2011; Arnold et al., 2013; Demuro et al., 2015). However, similar sized TT-OSL signal reductions have been observed over much shorter (<1 hour) daylight exposure times for some samples (Athanassas and Zacharias, 2010). TT-OSL depletion rates on the order of multiple days have also been reported from several solar simulator bleaching studies (e.g., Tsukamoto et al., 2008; Hernandez et al., 2012; Brown and Forman, 2012; Duval et al., 2017), albeit using different experimental conditions and simulated daylight intensities. In spite of these generally slow optical bleaching rates, equivalent dose (D_e) assessments performed on modern and very young samples suggest that adequate TT-OSL signal resetting down to sufficiently low levels is possible in some sedimentary environments. Multi-grain residual D_e values of 5-19 Gy have been reported for several modern aeolian sediments from Eurasia and South Africa (see Duller and Wintle, 2012). Arnold et al. (2014) reported a similarly sized multi-grain D_e of 7.3 ± 0.8 Gy for a modern slopewash and aeolian deposit from north-central Spain, while multi-grain residual D_e values of several tens of Gy have been obtained for coastal and lacustrine shoreline deposits from South Africa and Australia (Jacobs et al., 2011; Fu et al., 2017). In contrast, very large multi-grain TT-OSL residual doses of 250-300 Gy have been reported for modern suspended sediments and overbank deposits from the Yellow River (Hu et al., 2010), potentially cautioning against the suitability of TT-OSL dating in turbid and UV-depleted fluvial settings.

While these various TT-OSL bleaching assessments have proved insightful, they are based on a relatively modest number of observations (*n* = <20 samples) and further work is needed to better characterise TT-OSL signal resetting across a broader range of natural contexts using complementary types of experimental procedures. Additionally, all existing assessments of TT-OSL bleaching characteristics, with the exception of one study (Fu et al., 2017), have been performed at the multi-grain scale of D_e analysis. It remains unclear, therefore, whether TT-OSL residual doses reported in existing modern analogue studies partly reflect averaging effects arising from simultaneously measuring grains with different bleaching histories, signal compositions or TT-OSL source trap properties. For samples with inherently bright signal intensities, single-grain TT-OSL dating offers the potential to evaluate, or even circumvent, any potential averaging effects. Single-grain TT-OSL has recently been applied at several independently dated archaeological sites from Spain and Australia (e.g., Demuro et al., 2014; Arnold et al., 2015; Hamm et al., 2016). These single-grain studies have also revealed that multi-grain TT-OSL signals may be dominated by grains with unfavourable TT-OSL behaviours (e.g., Arnold and Demuro, 2015) and that apparent multi-grain TT-OSL residual doses of several tens of Gy may result from the inclusion of grain types that are routinely rejected by single-grain quality assurance criteria (Fu et al., 2017). Such complications require further examination, and additional single-grain bleaching assessments are needed to better characterise TT-OSL signal resetting at the most fundamental scale of D_e analysis.

The aims of the present study are threefold: (i) To examine the TT-OSL bleaching characteristics of quartz samples from a range of depositional environments using three complementary approaches; namely, daylight bleaching experiments, examination of modern sample D_e datasets, and comparisons of replicate TT-OSL and OSL ages for geological dating samples. The first two of these approaches permit examination of TT-OSL resetting properties under controlled bleaching conditions and in analogous natural depositional contexts, while the latter favours assessments of bleaching histories that are directly relatable to individual dating samples; (ii) To assess whether the bleaching properties of TT-OSL signals limit their dating applicability to certain depositional settings, environmental conditions or age ranges; (iii) To compare TT-OSL residual doses and bleaching trends at different scales of D_e analysis.

2. Sample details and experimental procedures

This study incorporates nineteen samples collected from a diverse range of depositional environments across Spain and Australia (**Fig. S1**). These two geographic regions have been targeted for their generally bright single-grain quartz TT-OSL signal characteristics (e.g., Arnold et al., 2015; Hamm et al., 2016), while individual sites within these regions have been selected to encompass a variety of natural bleaching conditions. Thirteen samples were collected from actively accumulating, or very recently accumulated, surface sediment deposits that were expected to yield burial doses close to, or consistent with, 0 Gy (assuming adequate signal bleaching during transportation). These samples represent modern analogues for associated archaeological, palaeontological and palaeoenvironmental dating samples being studied as part of recent or ongoing TT-OSL dating projects (e.g., Arnold et al., 2014; Demuro et al., 2014; Fu et al., 2017). Two shallow cave infill samples from the middle Pleistocene palaeoanthropological sites of Galería and Sima del Elefante, Atapuerca, (ATG10-3, ATE10-13) have been chosen for the daylight bleaching experiments, owing to their relatively high and comparable mean burial doses, and uniformly bleached single-grain TT-OSL D_e distributions (e.g., Demuro et al., 2014; Arnold et al., 2015). Single-grain TT-OSL and OSL dating comparisons were performed on four late Pleistocene samples from southern Kangaroo Island that exhibit different types of OSL D_e distributions, and that lie within typically routine OSL dating ranges (mean D_e values = 17-103 Gy). Two of these samples (KHC-KI5, KI14-5) were collected from relatively deep exogenous infill deposits preserved within Kelly Hill Cave (McDowell et al., 2013), and located ~25 m from the nearest palaeoentrance (Arnold et al., in prep). A third sample (KI14-12) was collected from a proximal (shallow) exogenous infill deposit preserved immediately beneath a former external opening of the same cave system. The fourth sample (KI14-1) was derived from a well-bedded coastal aeolianite deposit (Bridgewater Formation) found at the Boar Beach trace fossil site (Camens et al., 2017).

To achieve the main study aims, we have chosen to focus on single-grain TT-OSL and OSL analyses, which enable in depth assessments of bleaching adequacy in the absence of potential grain averaging effects. The details of the TT-OSL and OSL dating procedures employed in this study, including the quality assurance criteria used to eliminate unreliable grains, are provided in Arnold and Demuro

(2015), Arnold et al. (2016) and the Supporting Information (**Fig. S2-3**; **Table S1-3**). D_e values were determined for individual quartz grains using the single-aliquot regenerative-dose (SAR) procedures shown in **Table S1**. **Table S3** summarises the environmental dose rates for the Kangaroo Island dating samples, calculated using a combination of *in situ* field gamma-ray spectrometry (Arnold et al., 2012) and low-level beta counting (Bøtter-Jensen and Mejdahl, 1988).

3. TT-OSL daylight bleaching tests

To investigate the effects of controlled daylight exposure on single-grain TT-OSL D_e datasets, we bleached subsets of prepared quartz grains from samples ATG10-3 and ATE10-13 for 42 days on a south-facing exterior window ledge in Burgos, Spain. The original (unbleached) D_e datasets for these two samples exhibit relatively low overdispersion of 23-27%, and the majority of individual D_e estimates are consistent with single dose populations centred on central age model (CAM) D_e values of 540-572 Gy (**Fig. 1a-b**). The unlogged D_e dataset exhibit multiplicative D_e uncertainty properties (**Fig. S4**), and are normally distributed (ATG10-3) or slightly positively skewed (ATE10-13) according to the criterion outlined by Bailey and Arnold (2006) (**Table S4**).

After 6 weeks of daylight exposure, the weighted mean (CAM) D_e values for both samples were reduced by ~90% (**Fig. 1c-d**; **Table S4**). These depletion rates are consistent with that obtained for a multi-grain TT-OSL sample by Demuro et al. (2015) under analogous experimental conditions. Though both samples retain weighted mean (unlogged CAM; CAM_{UL}) residual D_e values of 54-65 Gy, complete resetting of burial doses is possible for a significant proportion of the measured grains in each sample. Between 38 and 52% of the daylight-bleached grains have D_e values consistent with 0 Gy at 2σ after 42 days of daylight exposure (**Table S4**). The D_e distributions are also characterised by higher overdispersion values of 49-57% and significantly enhanced positive skewness, and therefore appear to resemble heterogeneously bleached single-grain D_e datasets (e.g., Olley et al., 2004; Arnold et al., 2009).

It is difficult to determine whether these heterogeneous D_e distribution characteristics reflect genuine inter-grain differences in TT-OSL signal depletion rates or whether they are a reflection of pre-existing inter-grain differences in natural D_e values prior to bleaching. The former interpretation may be supported by published evidence suggesting that (i) TT-OSL signals are composites of multiple signal components with different detrapping probabilities (e.g., Tsukamoto et al., 2008; Brown and Forman, 2012; Demuro et al., 2015), and that (ii) inter-grain differences in TT-OSL behaviours (e.g., source traps and signal stabilities) are common in at least some samples (e.g., Arnold and Demuro, 2015; Duval et al., 2017; Bartz et al., this volume). Further support comes from **Table S4**, which shows that the higher overdispersion and enhanced skewness of the daylight-bleached datasets cannot be recreated by simply scaling the original D_e datasets by the average depletion rates measured in the bleaching experiments (0.11 ± 0.01 for ATG10-3 and 0.11 ± 0.01 for ATE10-13). It is also possible, however, that some of the enhanced overdispersion in the daylight-bleached D_e datasets may be caused by the increasing influence of intrinsic sources of D_e scatter over low dose ranges (e.g., different responses of individual grains to the SAR conditions). **Fig. S4** shows that the daylight-bleached D_e datasets exhibit distinctly different D_e uncertainty properties in comparison to the natural D_e datasets (additive rather than multiplicative D_e uncertainty relationships), reflecting the dominance of different types of experimental D_e scatter over low dose ranges.

4. Modern analogue D_e datasets

Ten of the thirteen modern samples yielded weighted mean (CAM_{UL}) single-grain OSL D_e values equivalent to 0 Gy at 2σ. Twelve of these samples also have OSL CAM_{UL} D_e values of <0.5 Gy and >80% of their measured grain populations yielded modern D_e values at 2σ (**Fig. 2-3**, **S5**, **Table S5**). These OSL datasets confirm that the collected samples are genuinely modern and have experienced at least several minutes of relatively homogenous daylight exposure prior to their recent deposition. The single-grain TT-OSL results for the modern samples are similarly encouraging, especially given the slower bleaching rates and non-zero Gy mean residual doses observed in the daylight bleaching experiments. Seven of the thirteen modern samples yield TT-OSL CAM$_{UL}$ D$_e$ values equal to 0 Gy at 2σ (**Table S5**). The majority of samples have TT-OSL CAM$_{UL}$ D$_e$ values <5 Gy; only three samples (LE14-MA1, CG12-M2 and FC15-MA1) have higher CAM$_{UL}$ D$_e$ values of 5-25 Gy (**Fig. 2**). The weighted mean residual D$_e$ for all thirteen samples is 3.8 ± 1.4 Gy for the TT-OSL datasets, compared to 0.01 ± 0.01 Gy for the OSL datasets. The SG TT-OSL$_{290}$ protocol, which is designed to maximise TT-OSL contributions from higher temperature source traps (Arnold and Demuro, 2015), yields CAM$_{UL}$ D$_e$ residuals that are statistically indistinguishable from their corresponding OSL and TT-OSL D$_e$ values at 2σ (**Table S5**, **Fig. 2**). Although only applied to four samples, the TT-OSL$_{290}$ signal therefore appears to be bleachable down to relatively low residual doses in some natural depositional contexts.

The TT-OSL D$_e$ distribution characteristics and weighted mean residual D$_e$ values vary significantly between sites from the same depositional setting (**Fig 2-3**), highlighting that it may not be appropriate to generalise about TT-OSL bleaching adequacy on the basis of depositional context alone. The single-grain TT-OSL D$_e$ distributions of all samples contain minor populations of high D$_e$ values when compared with their OSL counterparts (**Fig. 3**, **Fig. S5**). In some cases, the TT-OSL datasets exhibit more pronounced asymmetric tails of high D$_e$ values (**Fig. 3c**) and CAM$_{UL}$ overdispersion values of several Gy. However, all of the single-grain TT-OSL datasets contain significant populations (61-95%) of 'modern' grains that yield 0 Gy D$_e$ values at 2σ; **Table S5**, **Fig. 7**). For ten of the samples, the proportion of modern grains observed in the TT-OSL datasets are similar to (i.e., within 10% of) the proportions of modern grains recorded in the corresponding OSL datasets.

The modern analogue 'synthetic aliquot' D$_e$ datasets (equivalent to multi-grain aliquots containing 100-grains) reveal several interesting trends (**Fig. 2**, **Table S6**). The sample-averaged synthetic aliquot OSL residual D$_e$ is 0.67 ± 0.35 Gy for the thirteen samples, which is consistent with the sample-averaged single-grain OSL residual of 0.01 ± 0.01 Gy at 2σ. By contrast, the sample-averaged synthetic aliquot TT-OSL residual D_e (19.9 ± 4.3 Gy) exceeds its single-grain counterpart by a factor of five to six. Additionally, only one of the modern samples (ELC16-MA1) has a synthetic aliquot TT-OSL D_e value equal to 0 Gy at 2σ. The synthetic aliquot TT-OSL D_e values obtained in this study (0.3–63 Gy) overlap with multi-grain TT-OSL residual values reported elsewhere for modern analogues (e.g., Jacobs et al., 2011, Duller and Wintle, 2012; Arnold et al., 2014). For our datasets, comparisons undertaken at different scales of D_e analysis suggests that the systematically larger multi-grain TT-OSL residuals primarily arise from the inclusion of grain types that are rejected by the single-grain quality assurance criteria. There appears to be noticeable inter-sample variability in the types of rejected grains that exert strong multi-grain averaging effects, as might be expected for such a geographically diverse sample dataset. For instance, the presence of rejected grains with very slowly decaying TT-OSL signals appears to chiefly influence the multi-grain D_e results of samples CG12-M2 and LE14-MA1 (see also Tsukamoto et al., 2008; Demuro et al., 2015). For many of the other samples (e.g., FC16-MA1, ATD14-MA1, FM12-1), grains displaying anomalous dose-response properties or unsuitable recycling ratios appear to exert non-neutral effects on the final multi-grain D_e values.

5. Single-grain TT-OSL and OSL dating comparisons

The four Late Pleistocene dating samples from Kangaroo Island display different types of single-grain OSL D_e distributions (**Fig. 4**, **Table S3**), and therefore provide useful datasets for evaluating TT-OSL bleaching suitability across a range of dating contexts. Sample KI14-12, collected close to a cave palaeoentrance, yielded homogenous OSL and TT-OSL D_e datasets (**Fig. 4a**) with low overdispersion values of 17-19%, and indistinguishable CAM OSL and TT-OSL ages of 54.2–55.0 ka (**Table S3**). The consistency of these results supports the applicability of TT-OSL at this locality, and suggest that the Kelly Hill Cave infill deposits were exposed to prolonged daylight prior to entering the karst system.

Samples KHC-KI5 and KI14-5, collected from a deeper chamber within the same cave system, exhibit more heterogeneous OSL D_e distributions, higher overdispersion values of 30-37%, and their D_e datasets are better represented by the minimum age model (MAM) according to the maximum log likelihood criterion of Arnold et al. (2009) (**Fig. 4b-c**, **Table S3**). These complex D_e characteristics are interpreted as reflecting the entrainment of grains from pre-existing cave sediments during the transportation of predominantly well-bleached, externally derived sediments through the closed cave system (Arnold et al., in prep). The TT-OSL D_e datasets of these heterogeneously bleached samples exhibit pronounced residual D_e populations and higher overdispersion values than their OSL counterparts. In spite of their seemingly complicated depositional history, consistent TT-OSL and OSL ages of 16.1-18.2 ka and 67.3-67.7 ka were obtained for samples KHC-KI5 and KI14-5, respectively, using the MAM.

The OSL D_e dataset of sample KI14-1, collected from the Boar Beach fossil dune sequence, is characterised by low-to-moderate overdispersion and is well represented by the CAM according to its maximum log likelihood score (**Fig. 4d**, **Table S3**). The corresponding TT-OSL D_e dataset of KI14-1 exhibits moderate overdispersion of 42% and a more noticeable tail of high D_e values, which could suggest that daylight exposure was not long enough to completely reset the TT-OSL signal of all grains prior to deposition. Though the MAM-4 is statistically favoured over the CAM for this dataset, the TT-OSL ages obtained using both age models (115.2 ± 7.9 ka and 138.2 ± 9.3 ka, respectively) are consistent with the corresponding OSL age of 137.4 ± 8.5 ka at 2σ (CAM data not shown in **Table S3**).

6. Discussion and conclusions

The results of this study provide several useful insights into TT-OSL dating bleaching characteristics at different scales of D_e analysis. Daylight bleaching tests confirm that ~6 weeks of exposure may be needed to reduce sample-averaged single-grain TT-OSL residuals to within 10% of background; though complete signal resetting is possible for up to 50% of individually measured grains over the same time period. The CAM_{UL} residual doses (-0.1–23.9 Gy) obtained across a range of modern environments are noteworthy given these relatively slow daylight bleaching rates. The favourable modern analogue bleaching results imply prolonged surface residence times at the sites considered here. Alternatively, the sediment samples may have experienced progressive attenuation of residual signals prior to final deposition via multiple cycles of erosion, transportation and re-deposition (see Stokes, 1992).

Importantly, the modern analogue residual doses observed in this study are relatively low in comparison to the natural dose range of interest for typical TT-OSL dating applications. Residual D_e values on the order of 10^{-1}–10^{1} Gy are unlikely to compromise single-grain TT-OSL applicability beyond existing uncertainties in most middle or early Pleistocene dating studies. These unbleached TT-OSL residuals may give rise to more significant systematic age offsets when dating Holocene or late Pleistocene samples, particularly at the multi-grain scale of analysis. However, the low single-grain residuals obtained for many of the modern samples, and the consistent OSL and TT-OSL ages observed for the Kangaroo Island samples, suggest potential for reliable TT-OSL dating over shorter timescales at some sites.

Our various bleaching assessments suggest that single-grain TT-OSL dating suitability is not necessarily limited to certain depositional environments, as is sometimes assumed. Significant variation exists in the magnitudes of modern residual doses recorded both within and between different sedimentary settings (**Fig. 2**). The consistency of comparative OSL and TT-OSL ages from Kangaroo Island also supports the applicability of single-grain TT-OSL dating in some relatively complex sedimentary contexts, as long as appropriate statistical age models are considered. Though these findings are promising, our empirical datasets are relatively limited, and there remains a need to undertake site-specific bleaching assessments in any TT-OSL dating study; especially those conducted in high-latitude settings and depositional environments not covered by our modern analogue dataset. A potentially useful approach for assessing bleaching adequacy might involve comparisons of ages or D_e values obtained with multiple luminescence signals that bleach at different rates. Such assessments have been widely used in post-IR IRSL studies (e.g., Murray et al., 2012), with parity in ages or D_e values being used to support adequate resetting of the slower bleaching signal, all things being equal. The results of our comparative TT-OSL and OSL dating study support those of Demuro et al. (2015; this volume), and suggest that such differential bleaching assessments could provide useful insights into single-grain TT-OSL suitability in routine dating applications.

Our modern analogue D_e datasets, together with those reported by Gliganic et al. (2017), provide useful constraints on the amount of overdispersion observed in well-bleached modern or very young samples from a diverse range of settings. Well-bleached modern samples, with CAM_{UL} D_e values of 0 Gy at 2σ, yield unlogged overdispersion values of 0.12 ± 0.05 Gy for single-grain OSL datasets and 1.4 ± 0.5 Gy for single-grain TT-OSL datasets (**Fig. S6a-b**, **Table S6**). In the absence of site-specific constraints on underlying overdispersion, these average values might provide useful first order approximations for the σ_b parameter of the unlogged minimum age model (MAM_{UL}) and finite mixture model (FMM_{UL}); which should be specified in Gy when analysing heterogeneously bleached or mixed single-grain datasets containing 0 Gy or negative D_e values. When applying the conventional (logged) MAM and FMM, it may also be worthwhile considering the typical single-grain TT-OSL overdispersion values reported so far for well-bleached and unmixed geological (non-modern) samples. These published D_e datasets yield a mean overdispersion value of 21 ± 2% (**Table S7**, **Fig. S6c**), which is consistent with that reported for 'ideal' single-grain OSL samples (20 ± 1%; Arnold and Roberts, 2009).

Finally, our results show that significant differences may be observed between single-grain and multi-grain TT-OSL bleaching residuals for some modern samples. Assessment of multi-grain TT-OSL bleaching characteristics may be complicated by averaging effects of unsuitable grain types that are routinely rejected in single-grain analysis, paralleling observations reported in some OSL dating studies (e.g., Demuro et al., 2013; Arnold et al., 2013). These results also reinforce the findings of Arnold and Demuro (2015), which showed that the summed (multi-grain) TT-OSL characteristics of samples may not necessarily be representative of TT-OSL-producing grains that are individually considered suitable for dating.

Acknowledgements

Financial support for this research was provided by Australian research Council (ARC) Future Fellowship project FT130100195, Discovery Early Career Researcher Award DE160100743, grant CGL2010-16821 from the Ministerio de Economía y Competitividad de España, and Marie Curie International Reintegration Grant PIRG08-GA-2010-276810. We thank the Sierra de Atapuerca research team (EIA) and the Junta de Castilla y León for site access, and scientific and logistic support. We also thank members of the Australian Speleological Federation for facilitating access to the Nullarbor cave sites.

Figure captions

Figure 1 Natural and daylight-bleached single-grain TT-OSL D_e distributions for samples ATG10-3 and ATE10-13 from Atapuerca, Spain. Daylight bleaching experiments were conducted on monolayers of prepared quartz grains during July-August in Burgos, Spain (N 42^{o} 21’ 00” W 03^{o} 42’ 24”, 860 m.a.s.l.). The daylight-bleached grains were agitated every few days to ensure homogenous exposure of all grain surfaces during the 42 day bleaching period. The dark grey bands are centred on the weighted mean D_e values, which have been calculated using the CAM for the natural D_e datasets and the CAM_{UL} for the daylight-bleached D_e datasets. The light grey bands in plots (c) and (d) are centred on the target residual dose of 0 Gy. Radial plots (c) and (d) have been plotted using a modified log transformation of $z = log(D_e + a)$ (Galbraith and Roberts, 2012), to more easily accommodate both the large and small (negative and near zero Gy) D_e values observed in these datasets. The standard errors of these modified log transformed datasets are given relative to $D_e + a$, where a = 20 Gy for the daylight-bleached datasets of ATG10-3 and a = 30 Gy for the daylight-bleached dataset of ATE10-13.

Figure 2 (a) Single-grain TT-OSL, TT-OSL_{290} and OSL CAM_{UL} D_e values obtained for the modern analogue samples. (b) Synthetic aliquot TT-OSL, TT-OSL_{290} and OSL CAM_{UL} D_e values obtained for the modern analogue samples. Synthetic aliquot D_e values were obtained by summing the signals of all accepted and rejected grains types on each single-grain disc (equivalent to multi-grain aliquots containing 100-grains each). The dashed horizontal lines mark the expected D_e value (0 Gy) for these samples.

Figure 3 Representative modified log transformed radial plots showing single-grain TT-OSL and OSL D_e distributions for the modern analogue samples. See Figure 1 caption for details of the plotting procedure. An *a* offset value of 30 Gy was used to create plots (a) and (c). An *a* offset value of 40 Gy was used to create plot (b). The radial plots are centred on the expected D_e value of 0 Gy for each sample, while the light grey and dark grey bands are centred on the TT-OSL and OSL CAM_{UL} D_e values of each sample, respectively.

Figure 4 Paired single-grain TT-OSL and OSL D_e distributions for the Kangaroo Island dating samples, shown as radial plots. Each radial plot is centred on the TT-OSL CAM D_e value. The light grey and dark grey bands are centred on the TT-OSL and OSL D_e values used to calculate the final ages of each sample (see Table S3 for details).

References

Arnold, L.J., Roberts, R.G. 2009. Stochastic modelling of multi-grain equivalent dose (D_e) distributions: Implications for OSL dating of sediment mixtures. Quaternary Geochronology 4, 204-230.

Arnold, L.J., Demuro, M., 2015. Insights into TT-OSL signal stability from single-grain analyses of known-age deposits at Atapuerca, Spain. Quaternary Geochronology 30, 472-478.

Arnold, L.J., Roberts, R.G. Galbraith, R.F., DeLong, S.B. 2009. A revised burial dose estimation procedure for optical dating of young and modern-age sediments. Quaternary Geochronology 4, 306-325.

Arnold, L.J., Duval, M., Falguères, C., Bahain, J.-J., Demuro, M. 2012. Portable gamma spectrometry with cerium-doped lanthanum bromide scintillators: Suitability assessments for luminescence and electron spin resonance dating applications. Radiation Measurements 47, 6-18.

Arnold, L.J., Demuro, M., Navazo Ruiz, M., Benito-Calvo, A., Pérez-González, A., 2013. OSL dating of the Middle Palaeolithic Hotel California site, Sierra de Atapuerca, north-central Spain. Boreas 42, 285–305.

Arnold, L.J., Demuro, M., Parés, J.M., Arsuaga, J.L., Aranburu, A., Bermúdez de Castro, J.M., Carbonell, E., 2014. Luminescence dating and palaeomagnetic age constraint on hominins from Sima de los Huesos, Atapuerca, Spain. Journal of Human Evolution 67, 85-107.

Arnold, L.J., Demuro, M., Parés, J.M., Pérez-González, A., Arsuaga, J.L., Bermúdez de Castro, J.M., Carbonell, E., 2015. Evaluating the suitability of extended-range luminescence dating techniques over Early and Middle Pleistocene timescales: Published datasets and case studies from Atapuerca, Spain. Quaternary International 389, 167-190.

Arnold, L.J., Duval, M., Demuro, M., Spooner, N.A., Santonja, M., Pérez-González, A., 2016. OSL dating of individual quartz 'supergrains' from the Ancient Middle Palaeolithic site of Cuesta de la Bajada, Spain. Quaternary Geochronology 36, 78-101.

Athanassas, C., Zacharias, N., 2010. Recuperated-OSL dating of quartz from Aegean (South Greece) raised Pleistocene marine sediments: current results. Quaternary Geochronology 5, 65-75.

Bailey, R.M., and Arnold, L.J. 2006. Statistical modelling of single grain quartz De distributions and an assessment of procedures for estimating burial dose. Quaternary Science Reviews 25, 2475-2502.

Bartz, M., Arnold, L.J., Demuro, M., Duval, M., King, G.E., Rixhon, G., Álvarez Posada, C., Parés, J.M., Brückner, H., Quartz luminescence dating (multi-grain OSL and single-grain TT-OSL) confirms a Calabrian chronostratigraphy for the Lower Moulouya River deposits (NE Morocco). Quaternary geochronology, submitted (this volume).

Bøtter-Jensen, L., Mejdahl, M., 1988. Assessment of beta dose-rate using a GM multicounter system. Nuclear Tracks and Radiation Measurements 14, 187-191.

Brown, N.D., Forman, S.L., 2012. Evaluating a SAR TT-OSL protocol for dating fine-grained quartz within Late Pleistocene loess deposits in the Missouri and Mississippi river valleys, United States. Quaternary Geochronology 12, 87-97.

Camens, A.B., Carey, S.P., Arnold, L.J., 2017. Vertebrate trace fossils from the Late Pleistocene of Kangaroo Island, South Australia. Ichnos: An International Journal for Plant and Animal Traces 0, 1-20. DOI 10.1080/10420940.2017.1337633.

Demuro, M., Arnold, L.J., Froese, D.G., Roberts, R.G., 2013. OSL dating of loess deposits bracketing Sheep Creek tephra beds, northwest Canada: Dim and problematic single-grain OSL characteristics and their effect on multi-grain age estimates. Quatern. Geochronol. 15, 67–87.

Demuro, M., Arnold, L.J., Parés, J.M., Pérez-González, A., Ortega, A.I., Arsuaga, J.L., Bermúdez de Castro, J.M., Carbonell, E., 2014. New luminescence ages for the Galería Complex archaeological site: Resolving chronological uncertainties on the Acheulean record of the Sierra de Atapuerca, northern Spain. PLOS ONE 9, e110169.

Demuro, M., Arnold, L.J., Parés, J.M., Sala, R., 2015. Extended-range luminescence chronologies suggest potentially complex bone accumulation histories at the Early-to-Middle Pleistocene palaeontological site of Huéscar-1 (Guadix-Baza basin, Spain). Quaternary International 389, 191-212.

Demuro, M., Arnold, L.J., Aranburu, A., Gómez-Olivencia, A., Arsuaga, J.L., Single-grain OSL dating of the Middle Palaeolithic site of Galería de las Estatuas, Atapuerca (Burgos, Spain). Quaternary geochronology, submitted (this volume).

Duller, G.A.T., Wintle, A.G., 2012. A review of the thermally transferred optically stimulated luminescence signal from quartz for dating sediments. Quaternary Geochronology 7, 6-20.

Duval, M., Arnold, L., V. Guilarte, M. Demuro, M. Santonja and A. Pérez-Gonzalez., 2017. Electron Spin Resonance dating of optically bleached quartz grains from the Middle Palaeolithic site of Cuesta de la Bajada (Spain) using the multiple centres approach. Quaternary Geochronology 37, 82-96.

Fu, X., Cohen, T.J., Arnold, L.J., 2017. Extending the record of lacustrine phases beyond the last interglacial for Lake Eyre in central Australia using luminescence dating. Quaternary Science Reviews 162, 88-110.

Galbraith, R.F., Roberts, R.G., 2012. Statistical aspects of equivalent dose and error calculation and display in OSL dating: an overview and some recommendations. Quaternary Geochronology 11, 1-27.

Gliganic, L.A., Cohen, T.J., Meyer, M., Molenaar, A., 2017. Variations in luminescence properties of quartz and feldspar from modern fluvial sediments in three rivers. Quaternary Geochronology 41, 70-82.

Hamm, G., Mitchell, P., Arnold, L.J., Prideaux, G.J., Questiaux, D., Spooner, N.A., Levchenko, V.A., Foley, E.C., Worthy, T.H., Stephenson, B., Coulthard, V., Coulthard, C., Wilton, S., Johnston, D., 2016. Cultural innovation and megafauna interaction in the early settlement of arid Australia. Nature 539, 280-283.

Hernandez, M., Mauz, B., Mercier, N., Shen, Z., 2012. Evaluating the efficiency of TT-OSL SAR protocols. Radiation Measurements 47, 669-673.

Hu, G., Zhang, J.-F., Qiu, W.-L., Zhou, L.P., 2010. Residual OSL signals in modern fluvial sediments from the Yellow River (HuangHe) and the implications for dating young sediments. Quaternary Geochronology 5, 187-193.

Jacobs, Z., Roberts, R.G., Lachlan, T.J., Karkanas, P., Marean, C.W., Roberts, D.L., 2011. Development of the SAR TT-OSL procedure for dating Middle Pleistocene dune and shallow marine deposits along the southern Cape coast of South Africa. Quaternary Geochronology 6, 491-513.

McDowell, M.C., Bestland, E.A., Bertuch, F., Ayliffe, L.K., Hellstrom, J.C., Jacobsen, G.E., Prideaux, G., 2013. Chronology, stratigraphy and palaeoenvironmental interpretation of a Late Pleistocene to mid-Holocene cave accumulation on Kangaroo Island, South Australia. Boreas 42, 974-994.

Murray, A.S., Thomsen, K.J., Masuda, N., Buylaert, J.P., Jain, M., 2012. Identifying well-bleached quartz using the different bleaching rates of quartz and feldspar luminescence signals. Radiation Measurements 47, 688-695.

Olley, J.M., Pietsch, T., Roberts, R.G., 2004. Optical dating of Holocene sediments from a variety of geomorphic settings using single grains of quartz. Geomorphology 60, 337-358.

Stokes, S., 1992. Optical dating of young (modern) sediments using quartz: Results from a selection of depositional environments. Quaternary Science Reviews 11, 153-159.

Tsukamoto, S., Duller, G.A.T., Wintle, A.G., 2008. Characteristics of thermally transferred optically stimulated luminescence (TT-OSL) in quartz and its potential for dating sediments. Radiation Measurements 43, 1204-1218.

Wang, X.L., Wintle, A.G., Lu, Y.C., 2006. Thermally transferred luminescence in fine-grained quartz from Chinese loess: basic observations. Radiation Measurements 41, 649-658.

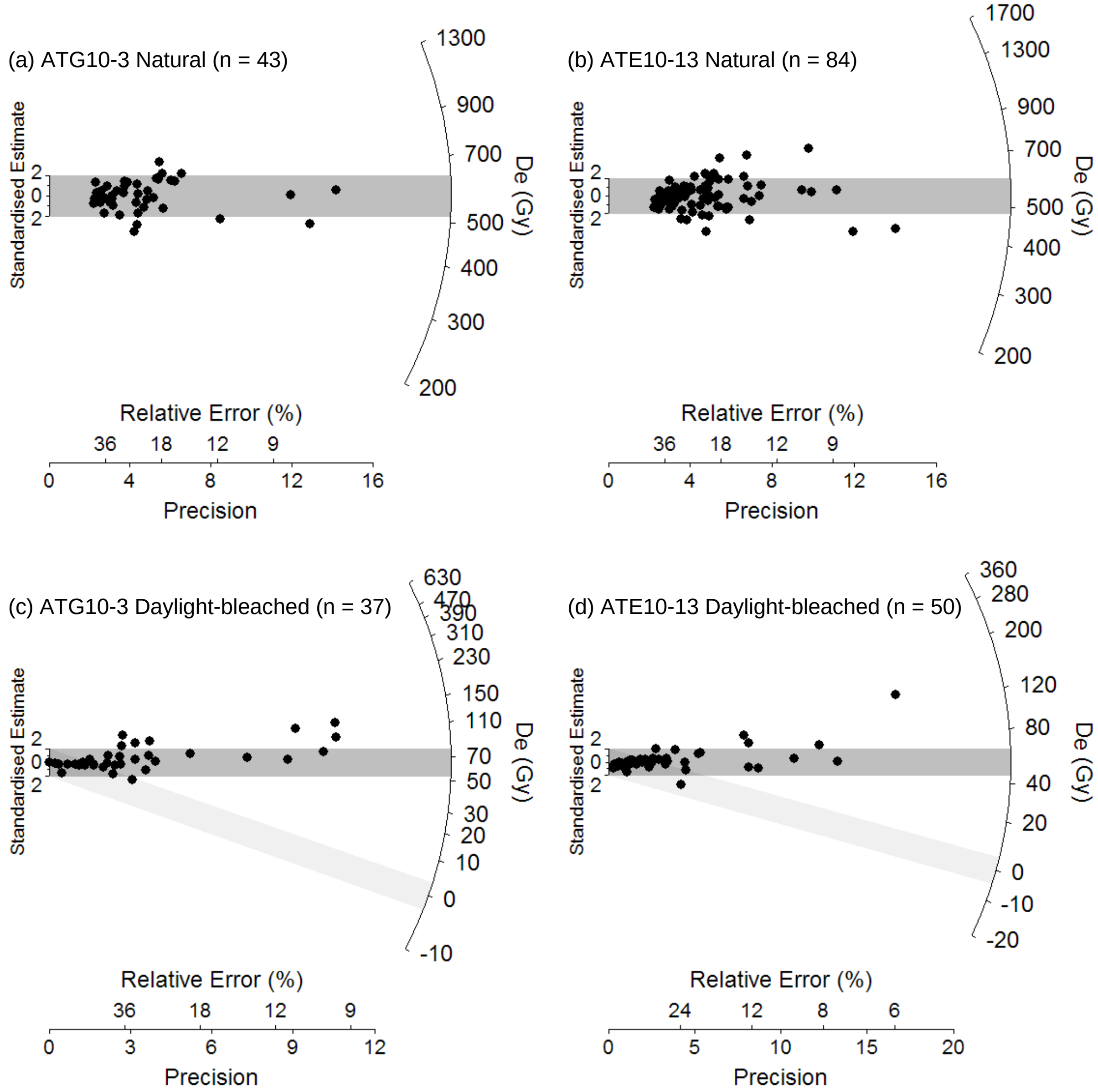
(a) ATG10-3 Natural (n = 43)
(b) ATE10-13 Natural (n = 84)
(c) ATG10-3 Daylight-bleached (n = 37)
(d) ATE10-13 Daylight-bleached (n = 50)
Standardised Estimate
De (Gy)
Relative Error (%)
Precision

Figure 1

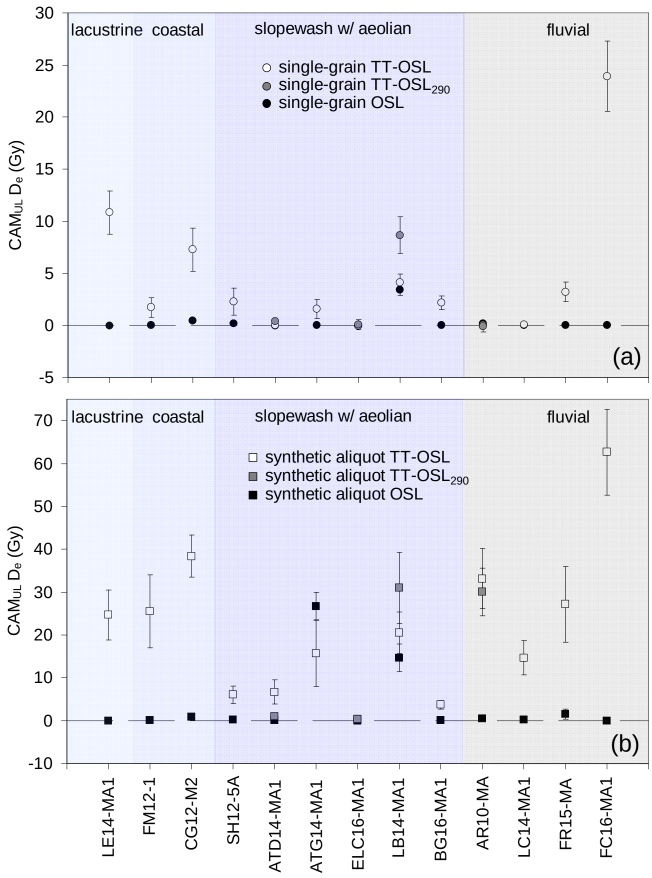
lacustrine
coastal
slopewash w/ aeolian
fluvial
single-grain TT-OSL
single-grain TT-OSL290
single-grain OSL
CAMUL De (Gy)
(a)
synthetic aliquot TT-OSL
synthetic aliquot TT-OSL290
synthetic aliquot OSL
(b)
LE14-MA1
FM12-1
CG12-M2
SH12-5A
ATD14-MA1
ATG14-MA1
ELC16-MA1
LB14-MA1
BG16-MA1
AR10-MA
LC14-MA1
FR15-MA
FC16-MA1

Figure 2

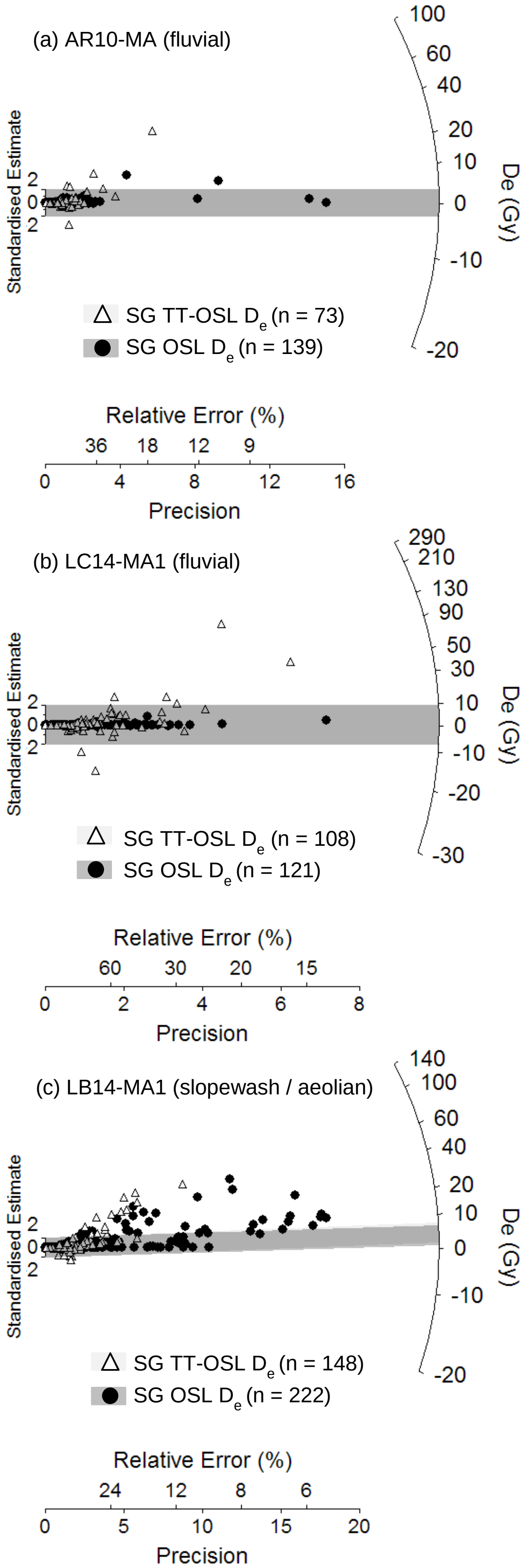
(a) AR10-MA (fluvial)
Standardised Estimate
De (Gy)
100
60
40
20
10
0
-10
-20
SG TT-OSL De (n = 73)
SG OSL De (n = 139)
Relative Error (%)
36 18 12 9
0 4 8 12 16
Precision
(b) LC14-MA1 (fluvial)
Standardised Estimate
De (Gy)
290
210
130
90
50
30
10
0
-10
-20
-30
SG TT-OSL De (n = 108)
SG OSL De (n = 121)
Relative Error (%)
60 30 20 15
0 2 4 6 8
Precision
(c) LB14-MA1 (slopewash / aeolian)
Standardised Estimate
De (Gy)
140
100
60
40
20
10
0
-10
-20
SG TT-OSL De (n = 148)
SG OSL De (n = 222)
Relative Error (%)
24 12 8 6
0 5 10 15 20
Precision

Figure 3

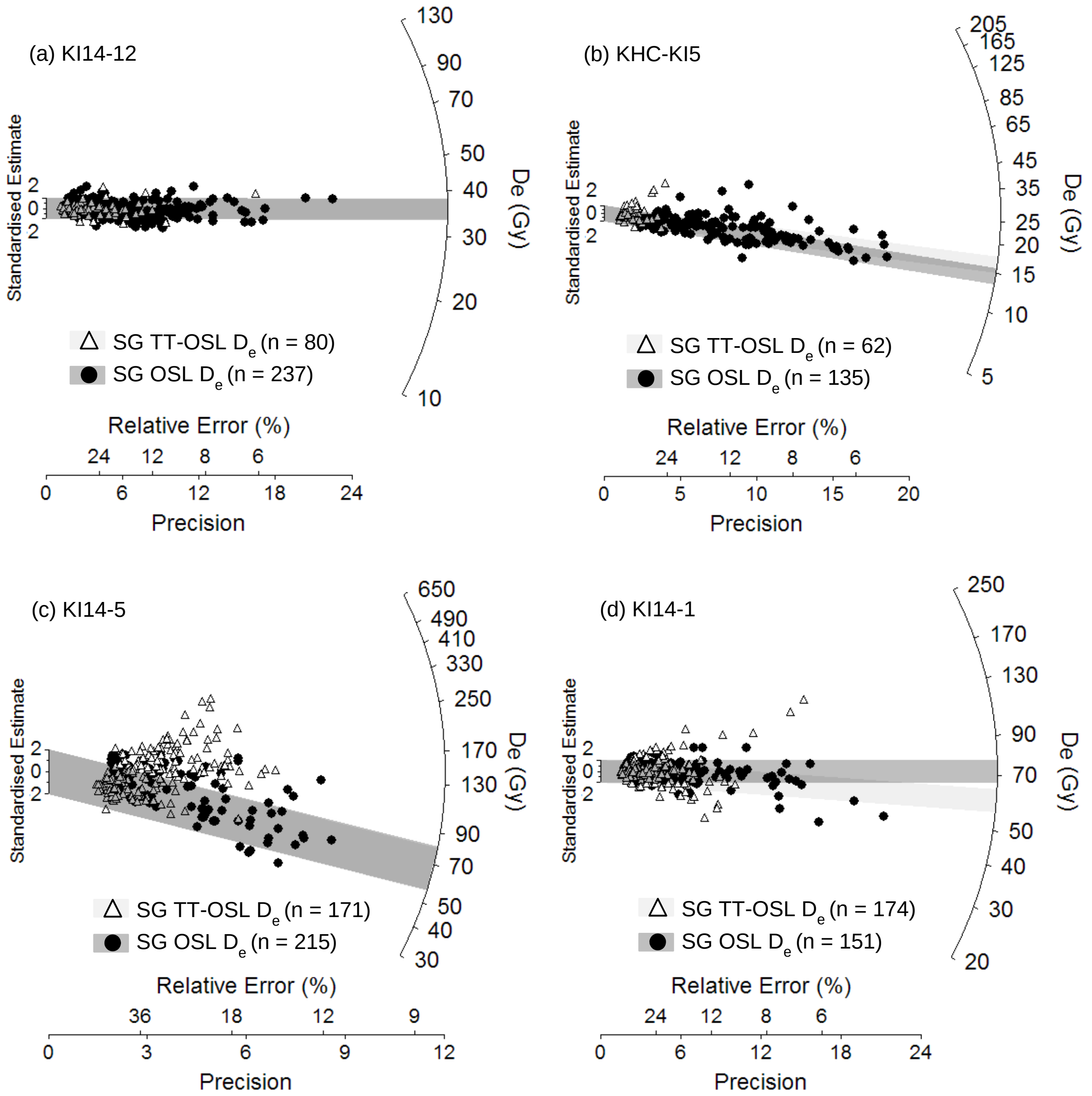
(a) KI14-12
Standardised Estimate
De (Gy)
SG TT-OSL De (n = 80)
SG OSL De (n = 237)
Relative Error (%)
Precision
(b) KHC-KI5
SG TT-OSL De (n = 62)
SG OSL De (n = 135)
(c) KI14-5
SG TT-OSL De (n = 171)
SG OSL De (n = 215)
(d) KI14-1
SG TT-OSL De (n = 174)
SG OSL De (n = 151)

Figure 4

Supplementary Information Arnold et al – Single-grain TT-OSL bleaching characteristics: Insights from modern analogues and OSL dating comparisons.

Single-grain TT-OSL and OSL dating protocols

The optical dating samples from Kangaroo Island (KI14-1, KI14-5, KI14-12, KHC-KI5) and Atapuerca (ATE10-13, ATG10-3) were collected by hammering PVC tubes into cleaned exposure faces, or by carefully extracting loose, unexposed sediment at night using filtered head torches. The Kangaroo Island samples were chosen for the single-grain OSL and TT-OSL dating comparison study because they displayed different types of single-grain OSL D_e distributions and because their natural D_e datasets lay within routine OSL dating ranges (mean D_e values = 17-103 Gy). Though single-grain TT-OSL dating is likely to offer few advantages over conventional single-grain OSL dating for such Late Pleistocene deposits, the Kangaroo Island samples are considered to be well-suited for this study as they permit comparative OSL assessments of TT-OSL bleaching adequacy in the absence of any potential OSL dose saturation effects.

The thirteen modern analogue samples were collected from the uppermost few cm of each surface deposit using a cleaned hand trowel or narrow PVC tube. These modern analogue samples represent contemporary or very recent (i.e., less than a few years old) transportation loads of depositional systems that are being dated as part of associated archaeological, palaeontological and palaeoenvironmental TT-OSL studies (e.g., Arnold et al., 2014, 2015, in prep; Demuro et al., 2014; Fu et al., 2017; Camens et al., 2017). In the case of the modern fluvial samples (AR10-MA, LC14-MA1, FR15-MA, FC16-MA1), the timing of the most recent depositional event is known to be <<10 years from oral and historical records, geomorphic mapping and satellite imagery. Aerial photography was also used to confirm that the surface lacustrine sediment sample from the southern margin of Lake Eyre North (LE14-MA1) was deposited during the well-documented 2010 flooding event, which occurred four years prior to sample collection. The five modern analogue samples collected adjacent to cave fossil site entrances (ATD14-MA1, ATG14-MA1, ELC16-MA1, LB14-MA1) and open-air fossil sites (BG16-MA1) comprise a mixture of slopewash and aeolian deposits. To ensure, as much as possible, that the sediments collected from these sites had been deposited within the last few years, we consulted with excavation teams that repeatedly visited the sites. We also specifically targeted actively accumulating surficial deposits that remained unvegetated and that had retained their original, undisturbed surface bedding features. The two littoral sediment samples (FM12-1, CG12-M2) were collected from modern beach foreshore deposits found within the current inter-tidal zone, and are thus considered to be contemporary in age. Collectively, the calculated burial doses of all thirteen modern or very recently deposited samples should, therefore, be consistent with, or very close to, an expected value of 0 Gy; assuming they have experienced adequate signal resetting prior to the most recent deposition cycle.

TT-OSL and OSL measurements were made on the 90-125, 180-250 or 212-250 μm quartz fractions using Risø TL-DA-20 readers equipped with blue LED units (470±20 nm, maximum power of 34 to 84 mW cm^{-2}), an array of infrared LEDs (peak emission 875 nm, maximum power of 130 to 151 mW cm^{-2}), and a 10 mW Nd:YVO_4 single-grain laser attachment emitting at 532 nm (maximum power of ~50 W cm^{-2}) (Thomsen et al., 2008). Ultraviolet OSL and TT-OSL signals were detected using EMI 9235QA photomultiplier tubes, fitted with 7.5 mm-thick Hoya U-340 filters. Samples were irradiated with mounted $^{90}Sr/^{90}Y$ beta sources that had been calibrated to administer known doses to multi-grain aliquots and single-grain discs. For single-grain measurements, spatial variations in beta dose rates across the disc plane were taken into account by undertaking hole-specific calibrations using gamma-irradiated quartz (Hansen et al., 2015).

Single-grain D_e estimates were measured using the single-aliquot regenerative dose (SAR) protocols shown in **Table S1a-c**. The single-grain TT-OSL SAR protocol (**Table S1a**) is based on the simplified multi-grain aliquot approach proposed by Stevens et al. (2009), and makes use of a TT-

OSL test dose (step 11) to correct for sensitivity change. It also includes four preheats of 260 ^{o}C for 10 s in each SAR cycle, and two high temperature OSL treatments (steps 6 and 12) to prevent TT-OSL signal carry over from previous regenerative dose (L_x) and test dose (T_x) measurement steps. The modified single-grain TT-OSL SAR protocol (TT-OSL_{290}) shown in **Table S1b** uses a preheat of 290^{o}C for 10 s, which is designed to favour TT-OSL production from higher temperature source traps. For consistency, all four preheat treatments (PH_1 to PH_4) were kept the same to mirror the original TT-OSL SAR D_e measurement protocol. This protocol was tested by Arnold and Demuro (2015) as a means of isolating (or maximising) TT-OSL contributions from higher temperature source traps for grains that display thermally unstable TT-OSL signals. It has been applied to a sub-set of the modern analogue samples to assess whether the TT-OSL_{290} signal from higher temperature source traps is readily bleachable in natural depositional contexts. The single-grain OSL SAR protocols adopted in this study make use of different preheat combinations for each sampling site, as detailed in **Table S1c**. The optimum preheat combination for each sample has been determined from site-specific dose-recovery tests (e.g., Arnold et al., 2012a, 2013, in prep, Fu et al., 2017; Camens et al., 2017), and corresponds to the conditions that yielded measured-to-given dose ratios consistent with unity at 2σ.

Single-grain D_e measurements were made using standard single-grain aluminium discs drilled with an array of 300 μm x 300 μm holes. Single-grain OSL measurements were made on either 180-250 or 212-250 μm quartz fractions, with the exception of samples SH12-5A and CG12-M2. These two samples contained insufficient fine sand yields, and so it was necessary to measure their 90-125 μm quartz fractions. It is expected that ~18 grains were placed in each grain-hole position of the standard-sized single-grain discs when measuring these 90-125 μm fractions (Arnold et al., 2012a). Single-grain TT-OSL measurements were made on equivalent grain-size fractions for each sample, with the exception of ATD14-MA1 and ATG14-MA1. Arnold et al. (2014) and Demuro et al (2014) have shown that the Atapuerca infill deposits contain relatively small proportions of TT-OSL-producing quartz grains. We have therefore chosen to measure the 90-125 μm fractions of these two samples to enhance the number of usable grains per disc while minimising any 'pseudo' single-grain averaging effects, following the findings of Demuro et al. (2013).

Sensitivity-corrected dose-response curves were constructed using the first 0.17 s of each TT-OSL or OSL stimulation after subtracting a mean background count obtained from the last 0.25 s of the TT-OSL or OSL signal. The single-grain TT-OSL dose-response curves are generally characterised by continued signal growth at high doses (10^2-10^3 Gy) and are typically well-represented by a single saturating exponential function (e.g., **Fig. S2**). The suitability of the single-grain TT-OSL SAR protocols have been assessed at the various study sites using dose-recovery tests. In all cases the measured-to-given dose ratios are consistent with unity at 2σ, supporting the general applicability of the TT-OSL SAR protocols. Further details of these TT-OSL dose-recovery test results can be found in related publications (e.g., Arnold et al., 2013, 2014, 2015, in prep; Demuro et al., 2014; Arnold and Demuro, 2015, Fu et al., 2017), and will be expanded upon in forthcoming site-specific studies. Representative examples of TT-OSL and OSL dose-recovery test results obtained for the dating comparison samples are shown in **Fig. S3**. A 40 Gy OSL dose-recovery test applied to 200 artificially bleached quartz grains of sample KHC-KI5 (bleached using 2 x 1000 s blue diode stimulation at 30 ^{o}C with a 10,000 s intervening pause) yielded an accurate measured-to-given dose ratio of 0.97 ± 0.03 with an overdispersion of 12 ± 4% (**Fig. S3a**). The TT-OSL dose-recovery test for KI14-12 (**Fig. S3b**) was performed on a batch of 200 unbleached grains owing to the longer exposure times needed to bleach natural TT-OSL signals down to low residual levels for all grains (see main text Section 3). A known (35 Gy) laboratory dose of similar magnitude to the expected D_e was added on top of the natural signal for these grains. The recovered dose was then calculated by subtracting the weighted mean natural D_e of sample KI14-12 (35.8 ± 1.4 Gy) from the weighted mean D_e of these unbleached and dosed grains (71.4 ± 4.1 Gy). This approach yielded a net (i.e., natural-subtracted) recovered-to-given ratio of 1.02 ± 0.06 and an overdispersion value of 21 ± 6% for the unbleached and dosed batch of grains.

Single-grain TT-OSL and OSL D_e estimates were only included in the final age calculations if they satisfied a series of standard quality assurance criteria (**Table S2**). Individual D_e estimates were rejected from further consideration if they exhibited one or more of the following properties: (i) weak TT-OSL or OSL signals (i.e., the net intensity of the natural test-dose signal, T_n, was less than three times the standard deviation of the late-light background signal); (ii) poor recycling ratios (i.e., the ratios of sensitivity-corrected luminescence response (L_x/T_x) for two identical regenerative doses were not consistent with unity at 2σ). In the case of the late Pleistocene dating samples from Kangaroo Island, the recycling ratio test was performed using both a low-dose and high-dose regenerative dose cycle (e.g., Arnold et al., 2016); (iii) high levels of signal recuperation (i.e., the sensitivity-corrected luminescence response of the 0 Gy regenerative-dose point amounted to >5% of the sensitivity-corrected natural signal response (L_n/T_n) at 2σ for geological dating samples or >0.1 Gy at 2σ for the modern analogue samples); (iv) anomalous dose-response curves (i.e., those displaying a zero or negative response with increasing dose) or dose-response curves displaying very scattered L_x/T_x values (i.e., those that could not be successfully fitted with the Monte Carlo procedure and, hence, did not yield finite D_e values and uncertainty ranges); (v) saturated or non-intersecting natural signals (i.e., L_n/T_n values equal to, or greater than, the I_{max} saturation limit of the dose-response curve at 2σ); (vi) extrapolated natural signals (i.e. L_n/T_n values lying more than 2σ beyond the L_x/T_x value of the largest regenerative-dose administered in the SAR procedure); (vii) contamination by feldspar grains or inclusions (i.e., the ratio of the L_x/T_x values obtained from two identical regenerative doses measured with and without prior IR stimulation (OSL IR depletion ratio; Duller, 2003) was less than unity at 2σ). For TT-OSL D_e estimation, criterion (vii) (feldspar contamination) was checked by measuring the OSL IR depletion ratio separately and in the standard manner for single-grain OSL measurements, i.e., by measuring two conventional single-grain OSL SAR cycles (as opposed to two single-grain TT-OSL SAR cycles) with and without IR stimulation.

The OSL, TT-OSL and TT-OSL_{290} grain classification statistics obtained for each sample after applying these quality assurance criteria are summarised in **Table S2**. In the case of samples LE14-MA1 and CG12-M2, a further 21 and 17 grains, respectively (1-2% of the total measured D_e values), were eliminated from the accepted single-grain TT-OSL D_e datasets because they exhibited very slow signal decay rates (i.e., their T_x signals did not reach background after 2 s of laser stimulation). Grains displaying such slow-dominated signals may not fulfil basic SAR suitability requirements (Wintle and Murray, 2006), and have been shown to be associated with thermally unstable signals, experimentally sensitised components or unreliable TT-OSL D_e estimates in several samples (e.g., Tsukamoto et al., 2008; Brown and Forman, 2012; Arnold and Demuro, 2015; Demuro et al., 2015; Bartz et al., submitted).

Individual D_e estimates are presented with their 1σ error ranges, which are derived from three sources of uncertainty: (i) a random uncertainty term arising from photon counting statistics for each TT-OSL measurement, calculated using Eq. 3 of Galbraith (2002); (ii) an empirically determined instrument reproducibility uncertainty of either 1.6%, 1.8%, 1.9% or 2.5% for each single-grain measurement (calculated for the specific Risø reader used for each sample using the approach outlined in Jacobs et al., 2006); and (iii) a dose-response curve fitting uncertainty determined using 1000 iterations of the Monte Carlo method described by Duller (2007) and implemented in Analyst.

Tables S3 summarise the environmental dose rate data for the Kangaroo Island dating samples. External gamma and beta dose rates have been calculated using a combination of *in situ* field gamma-ray spectrometry (Arnold et al., 2012b) and low-level beta counting of dried and homogenised, bulk sediments collected directly from the sampling positions (Bøtter-Jensen and Mejdahl, 1988). Cosmic-ray dose rate contributions were calculated using the equations of Prescott and Hutton (1994) after taking into consideration site altitude, geomagnetic latitude, and density, thickness and geometry of sediment and bedrock overburden. The beta, gamma and cosmic-ray dose rates have been corrected for long-term sediment moisture contents (Aitken, 1985), which are taken to be equivalent to the present-day measured water contents (Camens et al., 2017). A relative uncertainty of 25% (Kelly Hill Caves) and 20% (Boar Beach) has been assigned to the long-term moisture estimates to accommodate any minor variations in hydrologic conditions during burial. Dosimetry measurements were not made for the thirteen modern analogue samples because their age is already known to be less than a few years old, and the primary interest of this study was to determine the comparative magnitudes of TT-OSL and OSL residual D_e estimates in different types of depositional settings. We were also keen to avoid any time-dependent complications that might arise from calculating dose rates in progressively changing, near-surface dosimetric environments (Madsen and Murray, 2009).

References

Aitken, M.J., 1985. Thermoluminescence Dating. Academic Press, London, 359 p.

Arnold, L.J., Demuro, M., 2015. Insights into TT-OSL signal stability from single-grain analyses of known-age deposits at Atapuerca, Spain. Quaternary Geochronology 30, 472-478.

Arnold, L.J., Bailey, R.M., Tucker, G.E., 2007. Statistical treatment of fluvial dose distributions from southern Colorado arroyo deposits. Quaternary Geochronology 2, 162–167.

Arnold, L.J., Roberts, R.G. Galbraith, R.F., DeLong, S.B. 2009. A revised burial dose estimation procedure for optical dating of young and modern-age sediments. Quaternary Geochronology 4, 306-325.

Arnold, L.J., Demuro, M., Navazo Ruiz, M., 2012a. Empirical insights into multi-grain averaging effects from ‘pseudo’ single-grain OSL measurements. Radiation Measurements 47, 652–658.

Arnold, L.J., Duval, M., Falguères, C., Bahain, J.-J., Demuro, M. 2012b. Portable gamma spectrometry with cerium-doped lanthanum bromide scintillators: Suitability assessments for luminescence and electron spin resonance dating applications. Radiation Measurements 47, 6-18.

Arnold, L.J., Demuro, M., Navazo Ruiz, M., Benito-Calvo, A., Pérez-González, A., 2013. OSL dating of the Middle Palaeolithic Hotel California site, Sierra de Atapuerca, north-central Spain. Boreas 42, 285–305.

Arnold, L.J., Demuro, M., Parés, J.M., Arsuaga, J.L., Aranburu, A., Bermúdez de Castro, J.M., Carbonell, E., 2014. Luminescence dating and palaeomagnetic age constraint on hominins from Sima de los Huesos, Atapuerca, Spain. Journal of Human Evolution 67, 85-107.

Arnold, L.J., Demuro, M., Parés, J.M., Pérez-González, A., Arsuaga, J.L., Bermúdez de Castro, J.M., Carbonell, E., 2015. Evaluating the suitability of extended-range luminescence dating techniques over Early and Middle Pleistocene timescales: Published datasets and case studies from Atapuerca, Spain. Quaternary International 389, 167-190.

Arnold, L.J., Duval, M., Demuro, M., Spooner, N.A., Santonja, M., Pérez-González, A., 2016. OSL dating of individual quartz 'supergrains' from the Ancient Middle Palaeolithic site of Cuesta de la Bajada, Spain. Quaternary Geochronology 36, 78-101.

Bailey, R.M., and Arnold, L.J. 2006. Statistical modelling of single grain quartz De distributions and an assessment of procedures for estimating burial dose. Quaternary Science Reviews 25, 2475-2502.

Bartz, M., Arnold, L.J., Demuro, M., Duval, M., Klasen, N., King, G.E., Álvarez Posada, C., Parés, J.M., Rixhon, G., Brückner, H., Quartz luminescence dating (multiple-grain OSL and single-grain TT-OSL) confirms an early Pleistocene chronostratigraphy for the Lower Moulouya River (NE Morocco). Quaternary geochronology, submitted (this volume).

Bøtter-Jensen, L., Mejdahl, M., 1988. Assessment of beta dose-rate using a GM multicounter system. Nuclear Tracks and Radiation Measurements 14, 187-191.

Brown, N.D., Forman, S.L., 2012. Evaluating a SAR TT-OSL protocol for dating fine-grained quartz within Late Pleistocene loess deposits in the Missouri and Mississippi river valleys, United States. Quaternary Geochronology 12, 87-97.

Camens, A.B., Carey, S.P., Arnold, L.J., 2017. Vertebrate trace fossils from the Late Pleistocene of Kangaroo Island, South Australia. Ichnos: An International Journal for Plant and Animal Traces 0, 1-20. DOI 10.1080/10420940.2017.1337633.

Demuro, M., Arnold, L.J., Froese, D.G., Roberts, R.G., 2013. OSL dating of loess deposits bracketing Sheep Creek tephra beds, northwest Canada: Dim and problematic single-grain OSL characteristics and their effect on multi-grain age estimates. Quatern. Geochronol. 15, 67–87.

Demuro, M., Arnold, L.J., Parés, J.M., Pérez-González, A., Ortega, A.I., Arsuaga, J.L., Bermúdez de Castro, J.M., Carbonell, E., 2014. New luminescence ages for the Galería Complex archaeological site: Resolving chronological uncertainties on the Acheulean record of the Sierra de Atapuerca, northern Spain. PLOS ONE 9, e110169.

Demuro, M., Arnold, L.J., Aranburu, A., Gómez-Olivencia, A., Arsuaga, J.L., Single-grain OSL dating of the Middle Palaeolithic site of Galería de las Estatuas, Atapuerca (Burgos, Spain). Quaternary geochronology, submitted (this volume).

Duller, G.A.T., 2003. Distinguishing quartz and feldspar in single grain luminescence measurements. Radiation Measurements 37, 161–165.

Duller, G.A.T., 2007. Assessing the error on equivalent dose estimates derived from single aliquot regenerative dose measurements. Ancient TL 25, 15–24.

Fu, X., Cohen, T.J., Arnold, L.J., 2017. Extending the record of lacustrine phases beyond the last interglacial for Lake Eyre in central Australia using luminescence dating. Quaternary Science Reviews 162, 88-110.

Galbraith, R.F., 2002. A note on the variance of a background-corrected OSL count. Ancient TL 20, 49–51.

Galbraith, R.F., Roberts, R.G., Laslett, G.M., Yoshida, H., Olley, J.M., 1999. Optical dating of single and multiple grains of quartz from Jinmium rock shelter, northern Australia: part I, experimental design and statistical models. Archaeometry 41, 339-364.

Gliganic, L.A., Cohen, T.J., Meyer, M., Molenaar, A., 2017. Variations in luminescence properties of quartz and feldspar from modern fluvial sediments in three rivers. Quaternary Geochronology 41, 70-82.

Hamm, G., Mitchell, P., Arnold, L.J., Prideaux, G.J., Questiaux, D., Spooner, N.A., Levchenko, V.A., Foley, E.C., Worthy, T.H., Stephenson, B., Coulthard, V., Coulthard, C., Wilton, S., Johnston, D.,

2016. Cultural innovation and megafauna interaction in the early settlement of arid Australia. Nature 539, 280-283.

Hansen, V., Murray, A., Buylaert, J.-P., Yeo, E.-Y., Thomsen, K., 2015. A new irradiated quartz for beta source calibration. Radiat. Meas. 81, 123-127.

Jacobs, Z., Duller, G.A.T., Wintle, A.G., 2006. Interpretation of single-grain D_e distributions and calculation of D_e. Radiation Measurements 41, 264–277.

Madsen, A.T., Murray, A.S., 2009. Optically stimulated luminescence dating of young sediments: A review. Geomorphology 109, 3-16.

Ollé, A., Vergès, J.M., Rodríguez, X.P., Cáceres, I., Angelucci, D.E., Vallverdú, J., Demuro, M., Arnold, L.J., Falguères, C., Bennàsar, M., López-García, J.M., Blain, H-.A., Bañuls-Cardona, S., Burjachs, F., Expósito, I., López-Polín1, L., López-Ortega, E., 2016. The Middle Pleistocene site of La Cansaladeta (Tarragona, Spain): Stratigraphic and archaeological succession. Quaternary International 393, 137-157.

Prescott, J.R., Hutton, J.T., 1994. Cosmic ray contributions to dose rates for luminescence and ESR dating: large depths and long-term time variations. Radiation Measurements 23, 497–500.

Stevens, T., Buylaert, J.-P., Murray, A.S., 2009. Towards development of a broadly-applicable SAR TT-OSL dating protocol for quartz. Radiation Measurements 44, 639-645.

Thomsen, K.J., Murray, A.S., Jain, M., Bøtter-Jensen, L., 2008. Laboratory fading rates of various luminescence signals from feldspar-rich sediment extracts. Radiation Measurements 43, 1474–1486.

Tsukamoto, S., Duller, G.A.T., Wintle, A.G., 2008. Characteristics of thermally transferred optically stimulated luminescence (TT-OSL) in quartz and its potential for dating sediments. Radiation Measurements 43, 1204-1218.

Wintle, A.G., Murray, A.S., 2006. A review of quartz optically stimulated luminescence characteristics and their relevance in single-aliquot regeneration dating protocols. Radiation Measurements 41, 369-391.

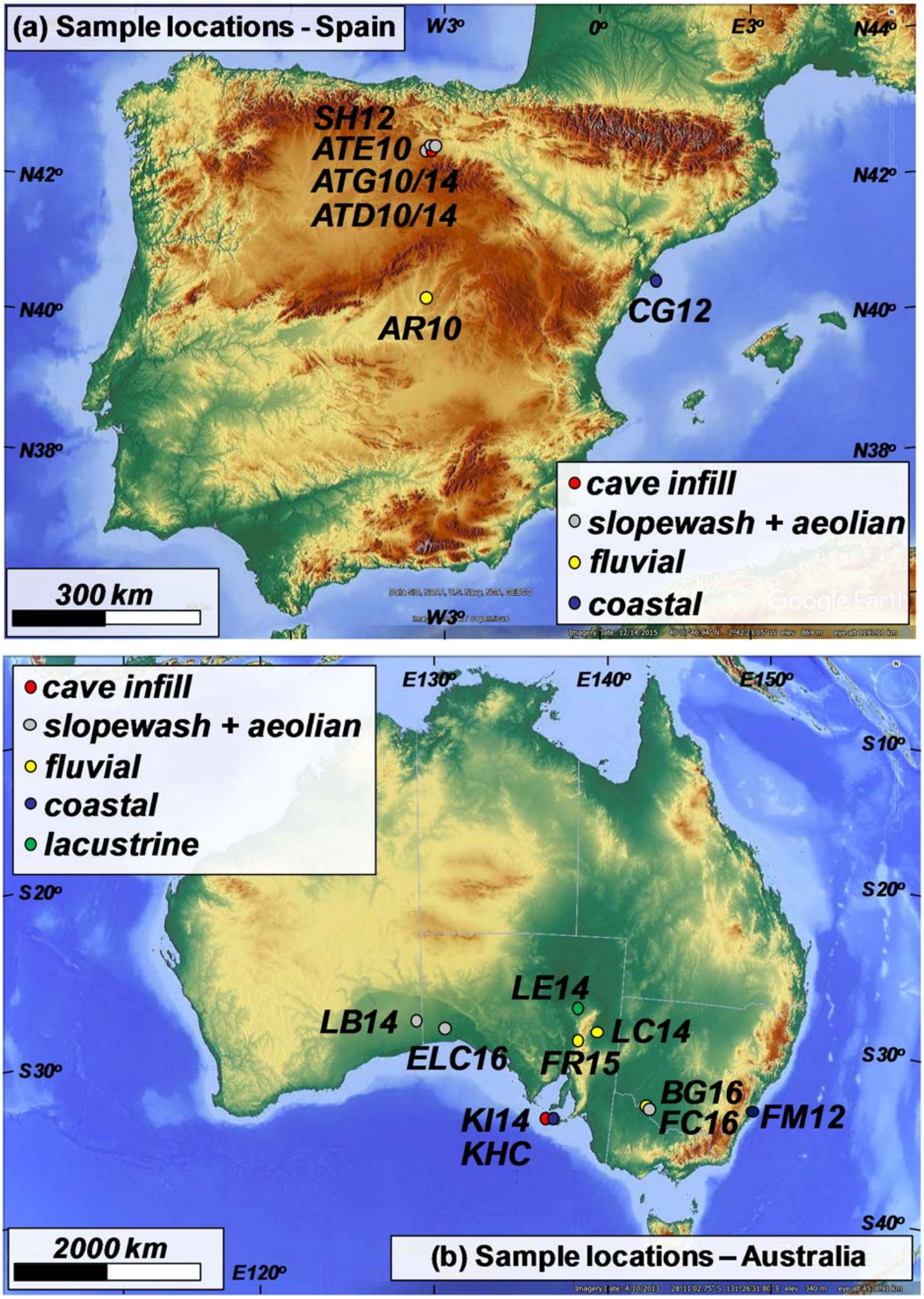

Figure S1 Topographic map of (a) the Iberian Peninsula and (b) Australia showing the location and type of sites considered in this study (source: Google Earth image with Maps-For-Free relief Overlay; http://ge-map-overlays.appspot.com/world-maps/maps-for-free-relief).

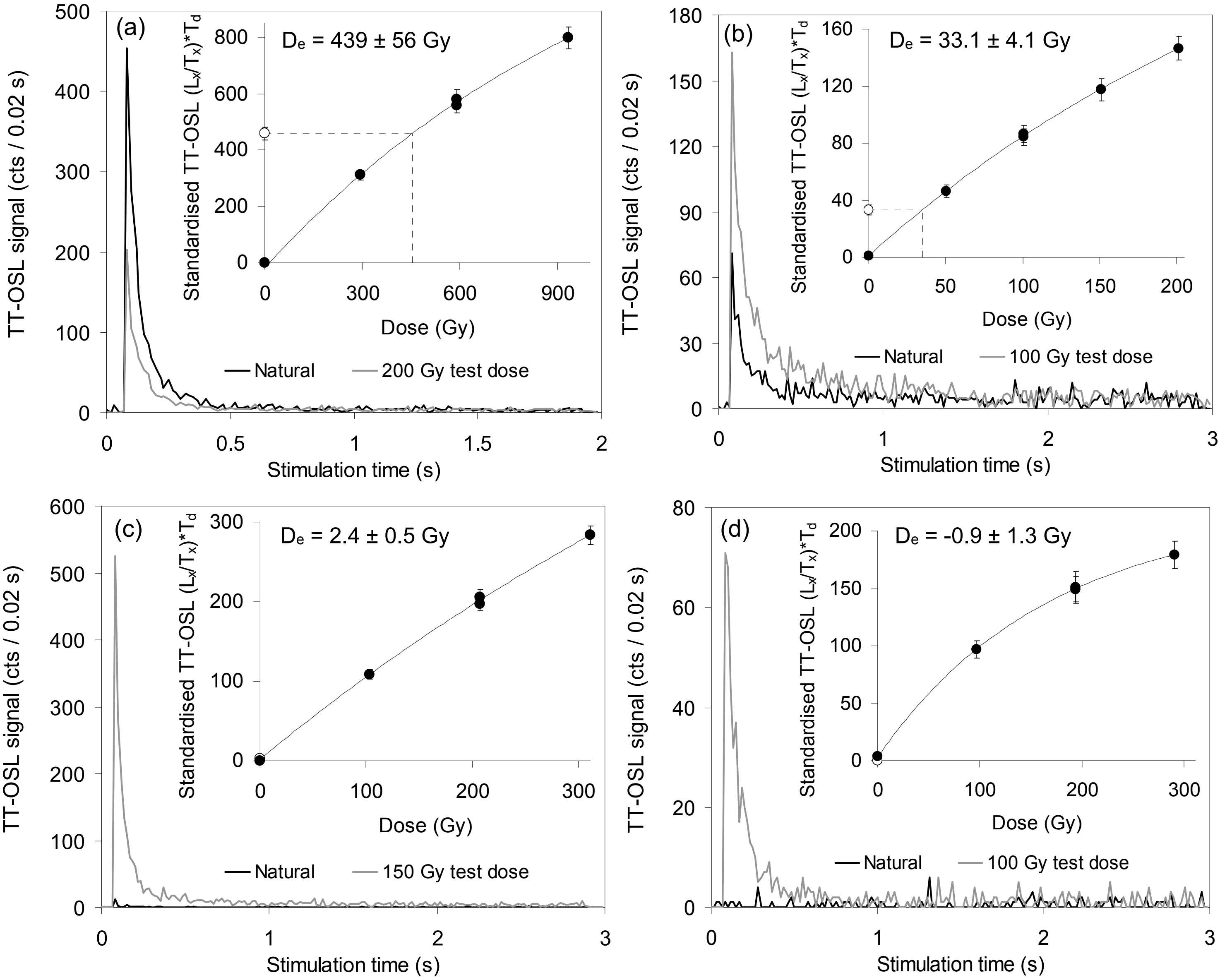

Figure S2 Representative single-grain TT-OSL decay and dose-response curves. In the insets, the open circle denotes the sensitivity-corrected natural OSL signal, and filled circles denote the sensitivity-corrected regenerated OSL signals. (a) Grain from sample ATG10-3 with a typical TT-OSL signal brightness (T_n ~500 counts / 0.17 s). (b) Grain from sample KI14-12 with a typical TT-OSL signal brightness (T_n ~500 counts / 0.17 s). (c) Grain from sample BG16-MA1 with a relatively bright TT-OSL signal (T_n ~1500 counts / 0.17 s). (d) Grain from sample ATG14-MA1 with a relatively dim TT-OSL signal (T_n ~250 counts / 0.17 s).

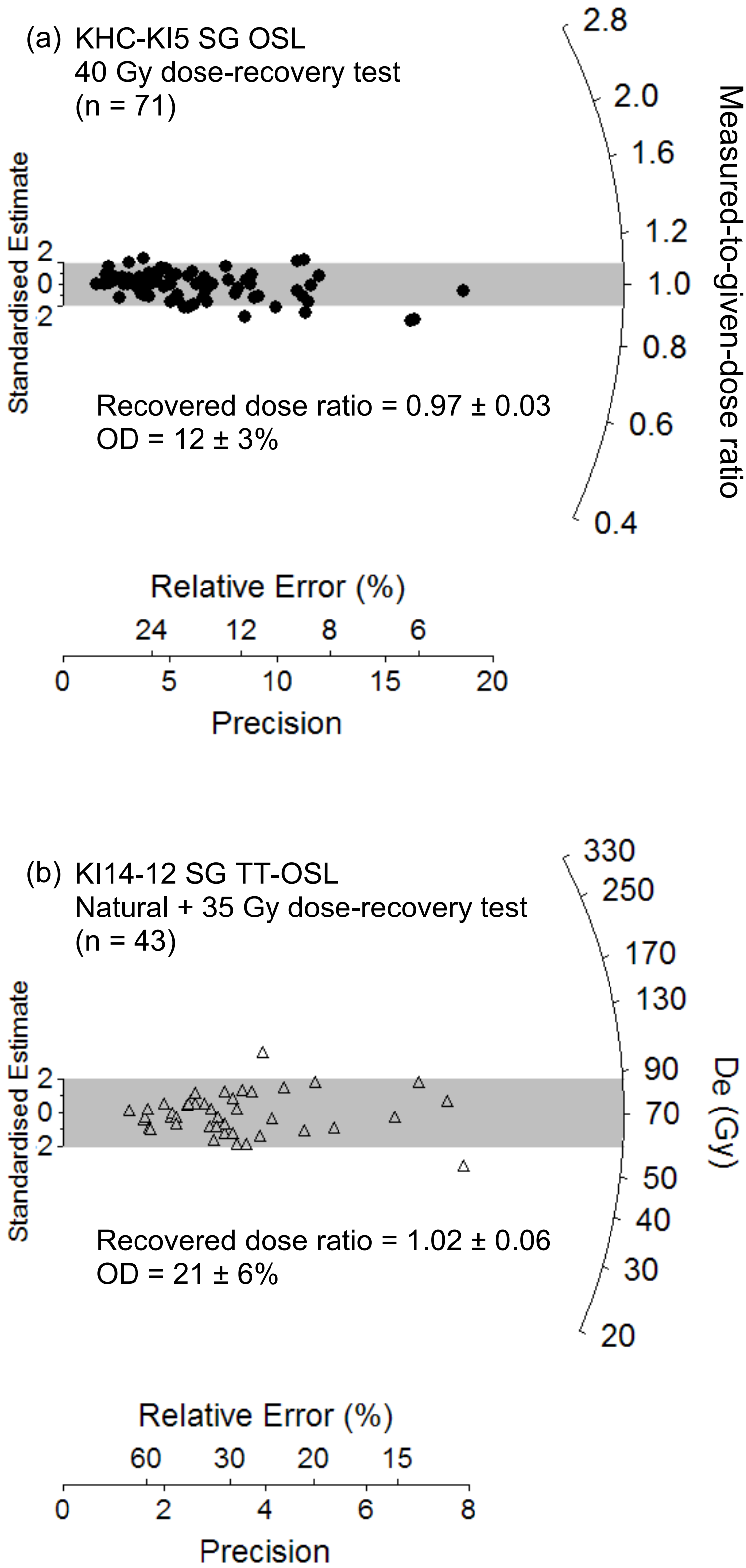

Figure S3 Radial plots showing single-grain OSL and TT-OSL dose-recovery test results for the Kangaroo Island dating samples. (a) Recovered-to-given dose ratios obtained for an OSL dose recovery test performed on individual quartz grains of sampleKHC-KI5. The grey shaded region on the radial plot is centred on the administered dose for each grain (recovered-to-given dose ratio of 1). (b) TT-OSL dose recovery test (natural + dosed) D_e values obtained for individual quartz grains of sample KI14-12. The grey shaded region on the radial plot is centred on the weighted mean D_e value.

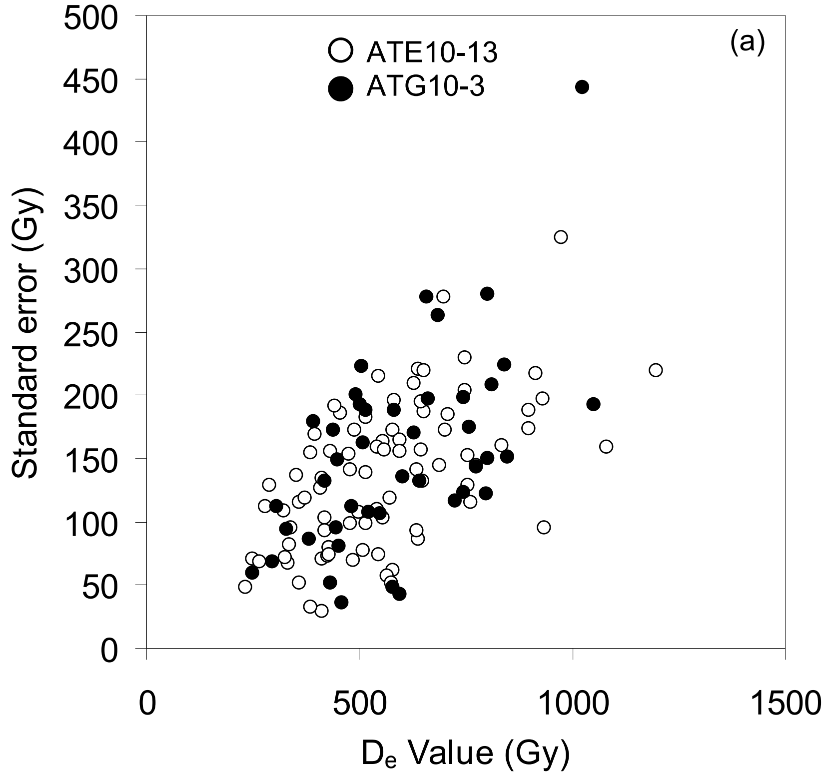

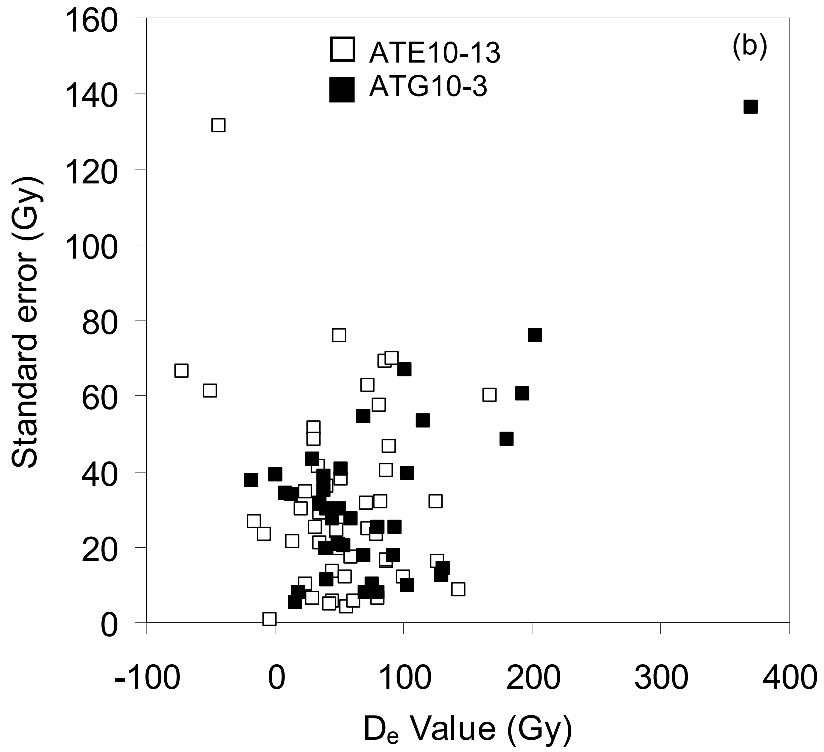

Figure S4 Plots of D_e versus standard error for the (a) natural and (b) daylight-bleached single-grain TT-OSL datasets of samples ATG10-3 and ATE10-13.

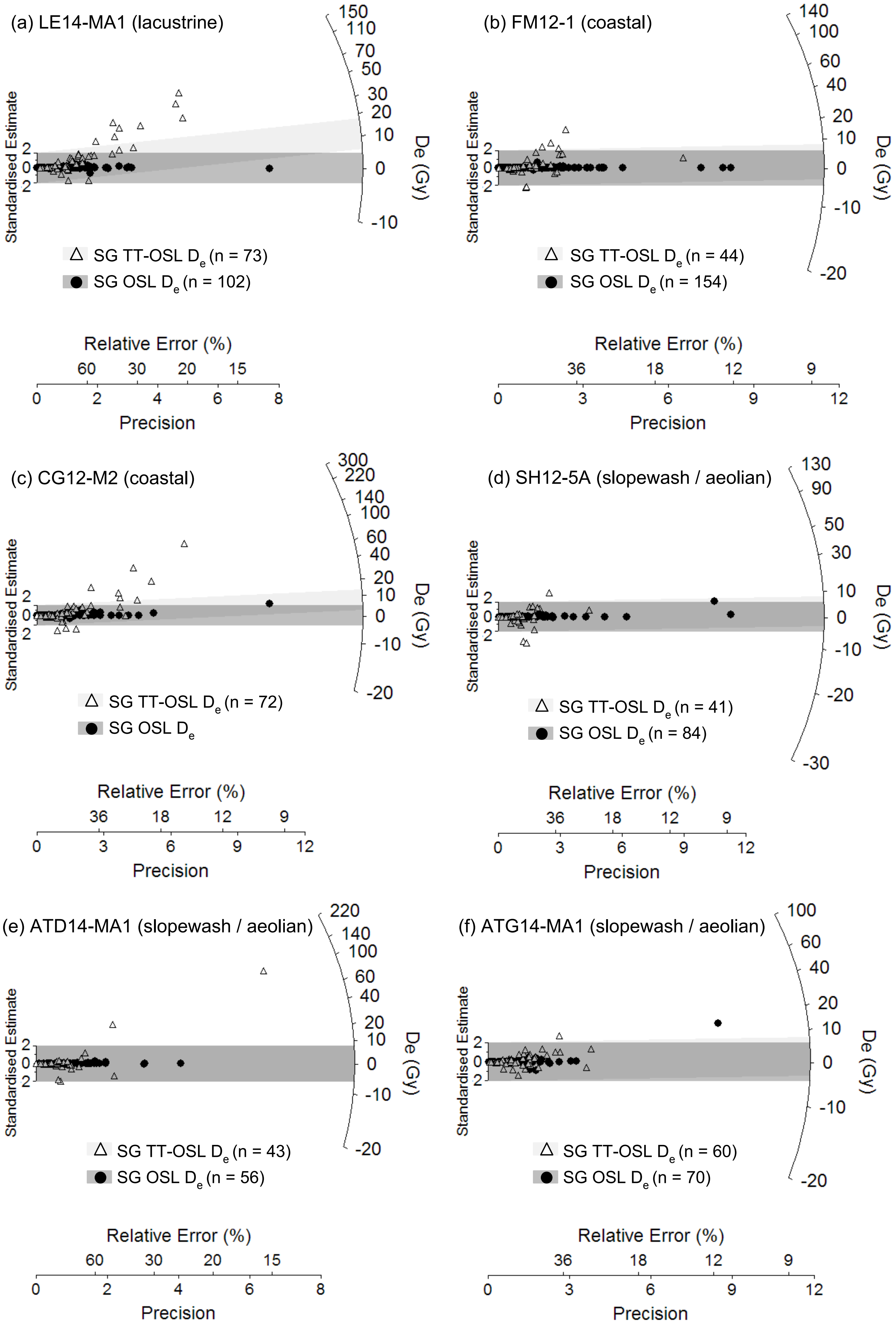
(a) LE14-MA1 (lacustrine)
Standardised Estimate
De (Gy)
SG TT-OSL D_e (n = 73)
SG OSL D_e (n = 102)
Relative Error (%)
Precision
(b) FM12-1 (coastal)
Standardised Estimate
De (Gy)
SG TT-OSL D_e (n = 44)
SG OSL D_e (n = 154)
Relative Error (%)
Precision
(c) CG12-M2 (coastal)
Standardised Estimate
De (Gy)
SG TT-OSL D_e (n = 72)
SG OSL D_e
Relative Error (%)
Precision
(d) SH12-5A (slopewash / aeolian)
Standardised Estimate
De (Gy)
SG TT-OSL D_e (n = 41)
SG OSL D_e (n = 84)
Relative Error (%)
Precision
(e) ATD14-MA1 (slopewash / aeolian)
Standardised Estimate
De (Gy)
SG TT-OSL D_e (n = 43)
SG OSL D_e (n = 56)
Relative Error (%)
Precision
(f) ATG14-MA1 (slopewash / aeolian)
Standardised Estimate
De (Gy)
SG TT-OSL D_e (n = 60)
SG OSL D_e (n = 70)
Relative Error (%)
Precision

Figure S5

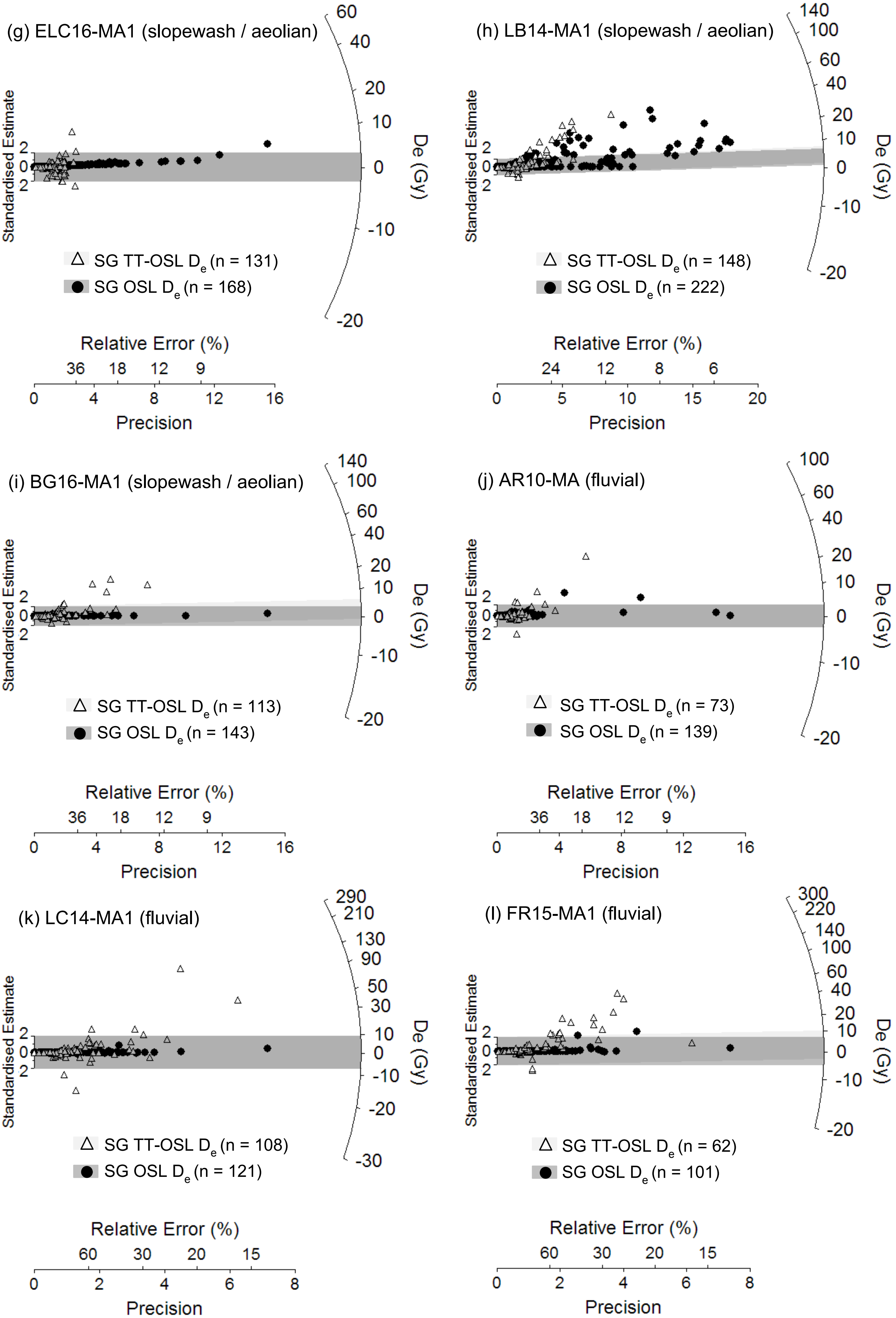
(g) ELC16-MA1 (slopewash / aeolian)
Standardised Estimate
De (Gy)
SG TT-OSL De (n = 131)
SG OSL De (n = 168)
Relative Error (%)
Precision
(h) LB14-MA1 (slopewash / aeolian)
SG TT-OSL De (n = 148)
SG OSL De (n = 222)
(i) BG16-MA1 (slopewash / aeolian)
SG TT-OSL De (n = 113)
SG OSL De (n = 143)
(j) AR10-MA (fluvial)
SG TT-OSL De (n = 73)
SG OSL De (n = 139)
(k) LC14-MA1 (fluvial)
SG TT-OSL De (n = 108)
SG OSL De (n = 121)
(l) FR15-MA1 (fluvial)
SG TT-OSL De (n = 62)
SG OSL De (n = 101)

Figure S5

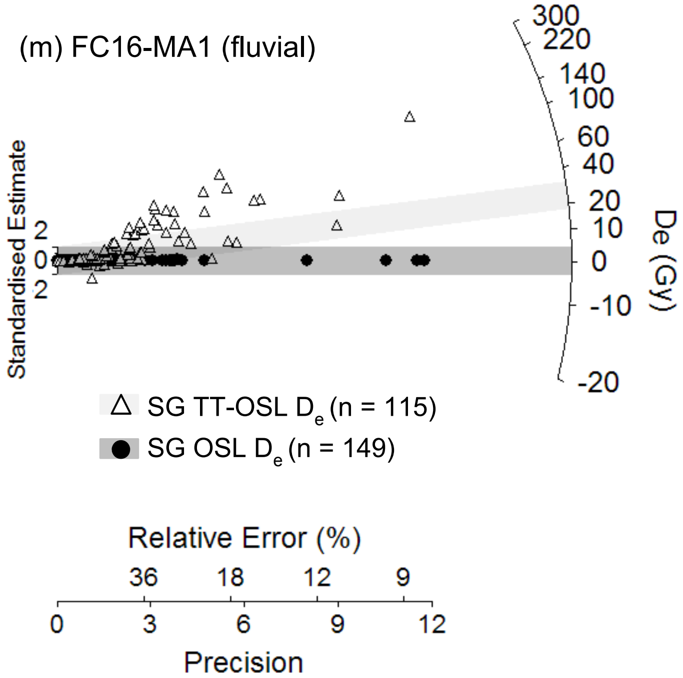

Figure S5 Modified log transformed radial plots showing single-grain TT-OSL and OSL D_e distributions for the modern analogue samples. See Figure 1 caption for details of the plotting procedure. An *a* offset value of 20 Gy was used to create plot (a), and an *a* offset value of 40 Gy was used to create plots (d) and (k). All other plots were created with an *a* offset value of 30 Gy. The radial plots are centred on the expected D_e value of 0 Gy for each sample, while the light grey and dark grey bands are centred on the TT-OSL and OSL CAM_{UL} D_e values of each sample, respectively.

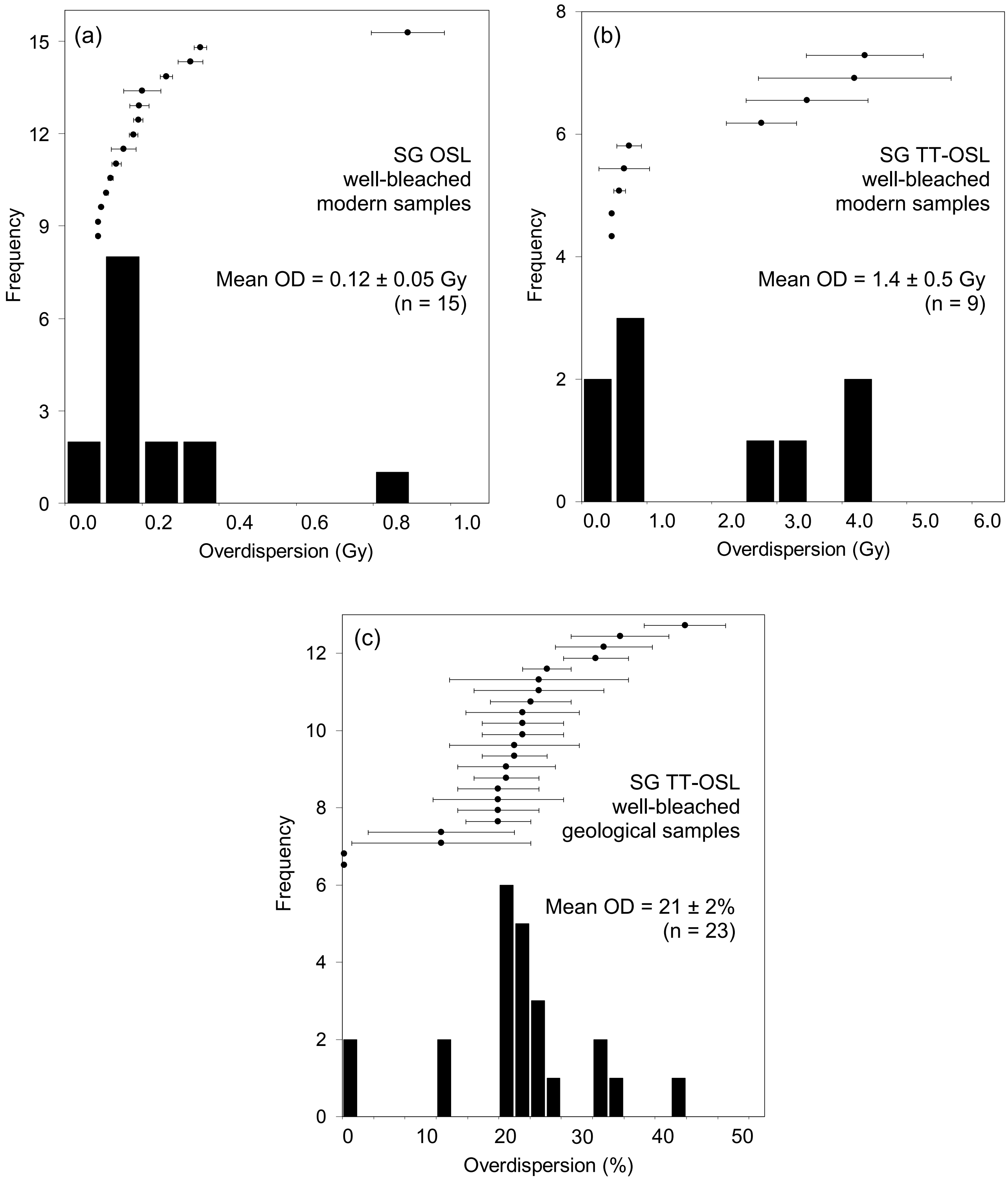

Figure S6 Frequency histograms showing the overdispersion values obtained for (i) well-bleached single-grain OSL modern samples (this study, Gliganic et al., 2017); (ii) well-bleached single-grain TT-OSL modern samples (this study); (iii) published well-bleached single-grain TT-OSL samples from (non-modern) geological and archaeological contexts. The overdispersion values shown in plots (a) and (b) have been calculated using the unlogged central age model (CAM_{UL}) and are given in Gy. The overdispersion values shown in plot (c) have been calculated using the logged central age model (CAM) and are given in %. The data used to create these plots are presented in **Table S6-S7**.

Table 2a: Single-grain TT-OSL SAR D_e protocol

Step	Treatment	Signal
1	Dose (natural or laboratory)	
2	Preheat 1 (PH_1 = 260ºC for 10 s)	
3	Single-grain OSL stimulation (125ºC for 2-3 s)	
4	Preheat 2 (PH_2 = 260ºC for 10 s)	
5	Single-grain TT-OSL stimulation (125ºC for 2-3 s)	L_n or L_x
6	OSL stimulation (280ºC for 400 s)	
7	Test dose (100-200 Gy)	
8	Preheat 3 (PH_3 = 260ºC for 10 s)	
9	Single-grain OSL stimulation (125ºC for 2-3 s)	
10	Preheat 4 (PH_4 = 260ºC for 10 s)	
11	Single-grain TT-OSL stimulation (125ºC for 2-3 s)	T_n or T_x
12	OSL stimulation (290 ºC for 400 s)	
13	Repeat measurement cycle for different sized regenerative doses	

Table 2a: Single-grain TT-OSL_{290} SAR D_e protocol

Step	Treatment	Signal
1	Dose (natural or laboratory)	
2	Preheat 1 (PH_1 = 290ºC for 10 s)	
3	Single-grain OSL stimulation (125ºC for 2-3 s)	
4	Preheat 2 (PH_2 = 290ºC for 10 s)	
5	Single-grain TT-OSL stimulation (125ºC for 2-3 s)	L_n or L_x
6	OSL stimulation (280ºC for 400 s)	
7	Test dose (100-200 Gy)	
8	Preheat 3 (PH_3 = 290ºC for 10 s)	
9	Single-grain OSL stimulation (125ºC for 2-3 s)	
10	Preheat 4 (PH_4 = 290ºC for 10 s)	
11	Single-grain TT-OSL stimulation (125ºC for 2-3 s)	T_n or T_x
12	OSL stimulation (290 ºC for 400 s)	
13	Repeat measurement cycle for different sized regenerative doses	

Table 2c: Single-grain OSL SAR D_e protocol

Step	Treatment	Signal
1	Dose (natural or laboratory)	
2	IRSL stimulation (50ºC for 60 s) [a]	
3	Preheat 1 (variable ºC for 10 s) [b]	
4	Single-grain OSL (125ºC for 2 s)	L_x
5	Test dose (5-10 Gy)	
6	Preheat 2 (variable ºC for 10 s) [b]	
7	Single-grain OSL (125ºC for 2 s)	T_x
8	Repeat measurement cycle for different sized regenerative doses	

[a] Step 2 is only included in the single-grain SAR procedure when measuring the OSL IR depletion ratio (Duller, 2003).
[b] The following PH_1 and PH_2 combinations were used for OSL D_e measurements in this study: FM12-1, LB14-MA1, ELC16-MA1, LE14-MA1, CG12-M2 – PH_1 = 260 ºC, 10 s, PH_2 = 160 ºC, 10 s; FR15-MA, LC14-MA1 – PH_1 = 240 ºC, 10 s, PH_2 = 160 ºC, 10 s; BG16-MA1, FC16-MA1 – PH_1 = 240 ºC, 10 s, PH_2 = 180 ºC, 10 s; AR10-MA – PH_1 = 240 ºC, 10 s, PH_2 = 200 ºC, 10 s; KI14-12, KI14-1, KHC-KI5, KI14-5 – PH_1 = 260 ºC, 10 s, PH_2 = 200 ºC, 10 s; ATG14-MA1, ATD14-MA1, SH12-5A – PH_1 = 200 ºC, 10 s, PH_2 = 200 ºC, 10 s;

Table S1 SAR protocols used for single-grain TT-OSL, TT-OSL_{290} and OSL D_e determination. For each protocol, the SAR measurement cycle was repeated for the natural dose, three to four different sized regenerative doses, a 0 Gy regenerative dose (to measure OSL signal recuperation) and a replicate of the lowest regenerative dose cycle (to assess the suitability of the test dose sensitivity correction). For some samples (see **Table S2**), the highest regenerative dose cycle of the single-grain OSL SAR protocol was also repeated to test the suitability of the test dose sensitivity correction over the high dose range of the dose-response curve. For the TT-OSL and TT-OSL_{290} SAR protocols, the OSL IR depletion ratio of Duller (2003) was measured separately and used to check for the presence of feldspar contaminants. The TT-OSL_{290} SAR D_e protocol used a $PH_{1\text{-}4}$ of 290ºC for 10 s, which was chosen as corresponding with peak TT-OSL production in the study of Arnold and Demuro (2015). L_x = regenerative dose signal response; L_n = natural dose signal response; T_x = test dose signal response for a laboratory dose cycle T_n = test dose signal response for the natural dose cycle.

Sample name	ATG10-3	ATG10-3	ATE10-13	ATE10-13	KI14-12	KI14-12	KHC-KI5	KHC-KI5	KI14-5
SAR measurement type	TT-OSL Natural	TT-OSL Daylight-bleached	TT-OSL Natural	TT-OSL Daylight-bleached	TT-OSL	OSL	TT-OSL	OSL	TT-OSL
Total measured grains	800	400	1400	1000	400	900	500	400	1000
Reason for rejecting grains from D_e analysis									
Standard SAR rejection criteria:	%	%	%	%	%	%	%	%	%
T_n <3σ background	65	69	70	68	30	19	58	27	48
Low-dose recycling ratio ≠ 1 at ±2σ	5	4	4	5	13	18	7	9	7
High-dose recycling ratio ≠ 1 at ±2σ	-	-	-	-	-	8	-	6	-
OSL-IR depletion ratios <1 at ±2σ	0	0	0	0	0	3	3	4	0
0 Gy L_x/T_x >5% L_n/T_n	<1	2	<1	1	<1	<1	<1	1	1
Non-intersecting grains (L_n/T_n > dose response curve saturation)	<1	0	0	0	<1	<1	<1	2	0
Saturated grains (L_n/T_n ≥ dose response curve I_{max} at ±2σ)	<1	0	0	0	0	0	0	2	0
Extrapolated grains (L_n/T_n > highest L_x/T_x at ±2σ)	0	0	0	0	0	4	0	5	0
Anomalous dose response / unable to perform Monte Carlo fit	23	16	20	21	36	20	19	10	27
Sum of rejected grains (%)	95	91	94	95	80	74	88	66	83
Sum of accepted grains (%)	5	9	6	5	20	26	12	34	17

Table S2

Sample name	KI14-5	KI14-1	KI14-1	LE14-MA1	LE14-MA1	FM12-1	FM12-1	CG12-M2	CG12-M2
SAR measurement type	OSL	TT-OSL	OSL	TT-OSL	OSL	TT-OSL	OSL	TT-OSL	OSL
Total measured grains	1500	1000	1000	1200	800	500	500	2000	2000
Reason for rejecting grains from D_e analysis									
Standard SAR rejection criteria:	%	%	%	%	%	%	%	%	%
T_n <3σ background	27	46	39	79	60	74	40	81	77
Low-dose recycling ratio ≠ 1 at ±2σ	24	9	10	3	9	8	9	4	6
High-dose recycling ratio ≠ 1 at ±2σ	9	-	5	-	-	-	-	-	2
OSL-IR depletion ratios <1 at ±2σ	3	3	2	0	4	0	8	0	2
0 Gy L_x/T_x >5% L_n/T_n	2	0	1	2	4	<1	3	0	<1
Non-intersecting grains (L_n/T_n > dose response curve saturation)	3	<1	3	0	0	0	0	0	0
Saturated grains (L_n/T_n ≥ dose response curve I_{max} at ±2σ)	<1	0	<1	0	0	0	0	0	0
Extrapolated grains (L_n/T_n > highest L_x/T_x at ±2σ)	6	0	3	0	0	0	0	0	0
Anomalous dose response / unable to perform Monte Carlo fit	11	25	22	10	10	9	9	11	6
Sum of rejected grains (%)	86	83	85	94	87	91	69	96	94
Sum of accepted grains (%)	14	17	15	6	13	9	31	4	6

Table S2 cont.

Sample name	**SH12-5A**	**SH12-5A**	**ATD14-MA1**	**ATD14-MA1**	**ATD14-MA1**	**ATG14-MA1**	**ATG14-MA1**	**ELC16-MA1**	**ELC16-MA1**
SAR measurement type	TT-OSL	OSL	TT-OSL	$TT\text{-}OSL_{290}$	OSL	TT-OSL	OSL	TT-OSL	$TT\text{-}OSL_{290}$
Total measured grains	300	500	500	600	400	600	500	300	200
Reason for rejecting grains from D_e analysis									
Standard SAR rejection criteria:	%	%	%	%	%	%	%	%	%
T_n <3σ background	65	59	69	68	68	55	59	5	12
Low-dose recycling ratio ≠ 1 at ±2σ	5	8	16	11	6	10	9	29	18
High-dose recycling ratio ≠ 1 at ±2σ	-	-	-	-	-	-	-	-	-
OSL-IR depletion ratios <1 at ±2σ	0	5	0	0	4	0	3	0	0
0 Gy L_x/T_x >5% L_n/T_n	0	2	2	<1	1	1	3	2	7
Non-intersecting grains (L_n/T_n > dose response curve saturation)	0	0	0	0	0	0	1	0	0
Saturated grains (L_n/T_n ≥ dose response curve I_{max} at ±2σ)	0	0	0	0	0	0	0	0	0
Extrapolated grains (L_n/T_n > highest L_x/T_x at ±2σ)	0	0	0	0	0	0	0	0	0
Anomalous dose response / unable to perform Monte Carlo fit	16	9	4	13	7	24	11	20	22
Sum of rejected grains (%)	86	83	91	92	86	90	86	56	59
Sum of accepted grains (%)	14	17	9	8	14	10	14	44	41

Table S2 cont.

Sample name	ELC16-MA1	LB14-MA1	LB14-MA1	LB14-MA1	BG16-MA1	BG16-MA1	AR10-MA	AR10-MA	AR10-MA
SAR measurement type	OSL	TT-OSL	OSL	$TT\text{-}OSL_{290}$	TT-OSL	OSL	TT-OSL	$TT\text{-}OSL_{290}$	OSL
Total measured grains	400	500	500	400	1000	500	2000	1000	1600
Reason for rejecting grains from D_e analysis									
Standard SAR rejection criteria:	%	%	%	%	%	%	%	%	%
T_n <3σ background	20	35	11	39	66	35	82	82	71
Low-dose recycling ratio ≠ 1 at ±2σ	9	15	26	13	6	7	5	4	6
High-dose recycling ratio ≠ 1 at ±2σ	-	-	-	-	-	4	-	-	5
OSL-IR depletion ratios <1 at ±2σ	6	0	6	0	0	3	0	0	5
0 Gy L_x/T_x >5% L_n/T_n	4	2	3	3	<1	2	<1	0	<1
Non-intersecting grains (L_n/T_n > dose response curve saturation)	0	0	<1	0	0	0	<1	0	0
Saturated grains (L_n/T_n ≥ dose response curve I_{max} at ±2σ)	0	0	0	0	0	0	0	0	0
Extrapolated grains (L_n/T_n > highest L_x/T_x at ±2σ)	0	0	0	0	0	0	0	0	0
Anomalous dose response / unable to perform Monte Carlo fit	19	18	10	25	17	20	9	11	4
Sum of rejected grains (%)	58	70	56	80	89	71	96	97	91
Sum of accepted grains (%)	42	30	44	20	11	29	4	3	9

Table S2 cont.

Sample name	**FR15-MA1**	**FR15-MA1**	**LC14-MA1**	**LC14-MA1**	**FC16-MA1**	**FC16-MA1**
SAR measurement type	OSL	TT-OSL	TT-OSL	OSL	TT-OSL	OSL
Total measured grains	500	900	1100	1000	1000	600
Reason for rejecting grains from D_e analysis						
Standard SAR rejection criteria:	%	%	%	%	%	%
T_n <3σ background	53	76	66	61	66	51
Low-dose recycling ratio ≠ 1 at ±2σ	11	6	6	9	5	5
High-dose recycling ratio ≠ 1 at ±2σ	-	-	-	-	-	2
OSL-IR depletion ratios <1 at ±2σ	5	0	0	7	0	3
0 Gy L_x/T_x >5% L_n/T_n	3	<1	<1	2	<1	3
Non-intersecting grains (L_n/T_n > dose response curve saturation)	0	0	0	0	<1	0
Saturated grains (L_n/T_n ≥ dose response curve I_{max} at ±2σ)	0	0	0	0	0	0
Extrapolated grains (L_n/T_n > highest L_x/T_x at ±2σ)	0	0	0	0	0	0
Anomalous dose response / unable to perform Monte Carlo fit	8	10	18	9	17	11
Sum of rejected grains (%)	80	93	90	88	89	75
Sum of accepted grains (%)	20	7	10	12	12	25

Table S2 Single-grain TT-OSL, TT-OSL_{290} and OSL classification statistics. The proportion of grains that were rejected from the final D_e estimation after applying the various SAR quality assurance criteria are shown in rows 6-14. For samples LE14-MA1 and CG12-M2, the anomalous dose response category includes 21 and 17 grains, respectively, that were eliminated from the accepted single-grain TT-OSL D_e datasets because they exhibited very slow signal decay rates (i.e., their T_x signals did not reach background after 2 s of laser stimulation).

Sample	Deposit	Depth (m)	Grain size (μm)	Water content (%) [a]	Environmental dose rate (Gy/ka)				Equivalent dose (D_e) data					Final age (ka) [e]
					Beta dose rate	Gamma dose rate	Cosmic dose rate	Total dose rate [b]	D_e type	Accepted/ measured	Overdis-persion (%)	Age model [c,d]	D_e (Gy)	
Kelly Hill Cave sand cone exposure:														
KI14-12	shallow cave infill	1.25	212-250	1±1	0.29±0.02	0.29±0.01	0.05±0.01	0.65±0.03	SG OSL	237/9000	17±2	CAM	35.3±0.6	54.2±3.0
									SG TT-OSL	80/400	19±4	CAM	35.8±1.4	55.0±3.6
Kelly Hill Cave K1-P1 excavation:														
KHC-KI5	deep cave infill	0.85	212-250	3±1	0.43±0.01	0.43±0.01	0.02±0.01	0.91±0.03	SG OSL	135/400	30±2	MAM-3	14.7±0.8	16.1±1.1
									SG TT-OSL	62/500	73±11	MAM-3	16.5±3.1	18.2±3.4
KI14-5	deep cave infill	1.75	212-250	6±2	0.45±0.03	0.46±0.01	0.02±0.01	0.96±0.04	SG OSL	215/1500	37±3	MAM-4	67.7±3.0	70.7±4.7
									SG TT-OSL	171/1000	51±4	MAM-4	67.3±7.1	70.2±8.1
Boar Beach trace fossil site:														
KI14-1	coastal dune	10.5	212-250	5±1	0.24±0.01	0.18±0.01	0.06±0.01	0.52±0.03	SG OSL	151/1000	25±2	CAM	71.6±2.0	137.4±8.5
									SG TT-OSL	174/1000	42±3	MAM-4	60.0±2.5	115.2±7.9

[a] Field water content, expressed as % of dry mass of mineral fraction, with an assigned relative uncertainty of ±25%.
[b] Total dose rate includes an assumed internal dose rate of 0.03 ± 0.01 Gy / ka.
[c] The MAM D_e estimates have been calculated after adding, in quadrature, a relative error of 15% to each individual D_e measurement error based on the underlying dose overdispersion observed in the single-grain dose-recovery tests and in the 'ideal' well-bleached and unmixed sample (sample KI14-12).
[d] Age model selection – The CAM was used to calculate the final SG OSL and TT-OSL D_e of KI14-12 as this sample had low overdispersion values consistent with those observed in the dose recovery datasets at 2σ; **Fig. S3**). The overdispersion value of the KI14-1 SG OSL dataset is similarly consistent with that of the well-bleached sample KI14-12 at 2σ. All other D_e datasets are interpreted as being heterogeneously bleached on the basis of their higher overdispersion values (inconsistent with KI14-12 at 2σ), complex geomorphic contexts (deep cave infill deposits) and the relatively slow bleaching rate of the TT-OSL signal (**Fig. 1**). The choice of whether to use the MAM-3 or MAM-4 has been made on statistical grounds using the maximum log likelihood score criterion outlined by Arnold et al. (2009).
[e] Total uncertainty includes a systematic component of ±2% associated with laboratory beta-source calibration.

Table S3 Single-grain TT-OSL and OSL D_e summary statistics, dose rates and final ages for the Kangaroo Island samples.

Sample	Site / deposit	Grain size (µm)	D_e type	Accepted/ measured	W-skew [a]	Critical skew [b]	Overdis-persion (%)	Modern Grains (%) [c]	Age model	D_e (Gy)	D_e depletion ratio [d]
ATG10-3	Galería GIIIb	90-125	Natural	43/800	0.38	±0.75	23±5	0	CAM	572±29	-
			Daylight bleached (42 days)	37/400	2.22	±0.81	49±9	38	CAM_{UL}	65±7	0.11±0.01
			Natural (scaled by D_e depletion ratio)	43/800	0.33	±0.75	20±6	0	CAM	65±3	-
ATE10-13	Elefante TE19	90-125	Natural	84/1400	0.85	±0.53	27±4	0	CAM	540±21	-
			Daylight bleached (42 days)	50/500	3.21	±0.69	57±9	52	CAM_{UL}	54±6	0.10±0.01
			Natural (scaled by D_e depletion ratio)	84/1400	0.82	±0.53	24±4	0	CAM	54±2	-

[a] Weighted skewness scores have been calculated on the original rather than log-transformed D_e values (using Eq. 14 of Bailey and Arnold, 2006) owing to presence of negative D_e values in the daylight-bleached datasets.
[b] Critical skewness scores have been calculated using Eq. 16 of Bailey and Arnold (2006). D_e distributions are considered to be significantly skewed if the weighted skewness value is greater than the corresponding critical skewness value. Critical skewness values are taken to be equivalent to twice the standard error of skewness score for single-grain D_e datasets (Bailey and Arnold, 2006; Arnold et al., 2007).
[c] Modern grains are defined as having a D_e value consistent with 0 Gy at 2σ.
[d] D_e depletion ratio = W-mean D_e of daylight bleached dataset / w-mean D_e of Natural dataset.

Table S4 Single-grain TT-OSL summary statistics for the natural and daylight-bleached D_e datasets of samples ATG10-3 and ATE10-13 from Atapuerca, Spain.

(a) Sample	Site	Setting	SG TT-OSL results		SG TT-OSL$_{290}$ results		SG OSL results	
			% modern grains [a]	CAM$_{UL}$ D_e (Gy)	% modern grains [a]	CAM$_{UL}$ D_e (Gy)	% modern grains [a]	CAM$_{UL}$ D_e (Gy)
LE14-MA1	Lake Eyre Williams Point, Australia	lacustrine	79.5	10.8 ± 2.1			96.1	**-0.02±0.02**
FM12-1	Fairy Meadow Beach, Australia	littoral	88.6	**1.7±0.9**			87.0	**0.02±0.01**
CG12-M2	Sitges Beach, Spain	littoral	81.9	7.3±2.1			90.6	0.46±0.16
SH12-5A	Cueva Mayor exterior, Atapuerca, Spain	slopewash / aeolian	92.7	**2.3±1.3**			81.0	0.18±0.07
ATD14-MA1	Gran Dolina exterior, Atapuerca, Spain	slopewash / aeolian	95.3	**0.02±0.11**	84.4	0.40±0.14	100.0	**-0.03±0.04**
ATG14-MA1	Galería exterior, Atapuerca, Spain	slopewash / aeolian	91.7	**1.6±0.9**			94.3	**0.04±0.03**
ELC16-MA1	Emu Leap Cave, Nullarbor Plains, Australia	slopewash / aeolian	94.7	**-0.06±0.12**	94.0	**0.07±0.49**	88.1	**-0.04±0.02**
LB14-MA1	Leana's Breath Cave, Nullarbor Plains, Australia	slopewash / aeolian	79.7	4.1±0.8	74.1	8.7±1.8	70.7	3.4±0.6
BG16-MA1	Bone Gulch, Murray River, Australia	Slopewash / aeolian	91.2	2.2±0.6			94.4	**-0.01±0.02**
AR10-MA	Arganda, Spain	fluvial	93.2	**0.02±0.18**	93.8	**-0.11±0.50**	92.1	**0.20±0.10**
LC14-MA1	Lake Callabonna, Australia	fluvial	91.7	**0.05±0.10**			88.4	**-0.01±0.03**
FR15-MA	Hookina Creek, Australia	fluvial	77.4	3.2±0.9			83.2	**0.02±0.01**
FC16-MA1	Fishermans Cliff, Murray River, Australia	fluvial	60.9	23.9±3.4			85.9	**0.02±0.01**

[a] Modern grains/aliquots are defined as having a D_e value consistent with 0 Gy at 2σ. A small number of samples have higher proportions of modern grains in their TT-OSL D_e datasets than in their corresponding OSL D_e datasets (SH12-5A, ELC16-MA1, LB14-MA1). These minor differences primarily reflects the larger 2σ uncertainty ranges of the individual TT-OSL D_e values in comparison to their OSL counterparts (see **Fig. S5**).

Table S5 (caption on next page)

(b)

Sample	Site	Setting	Synthetic aliquot TT-OSL CAM$_{UL}$ D_e (Gy)	Synthetic aliquot TT-OSL$_{290}$ CAM$_{UL}$ D_e (Gy)	Synthetic aliquot OSL CAM$_{UL}$ D_e (Gy)
LE14-MA1	Lake Eyre Williams Point, Australia	lacustrine	24.7±5.8		**-0.01±0.05**
FM12-1	Fairy Meadow Beach, Australia	littoral	25.5±8.5		**0.03±0.02**
CG12-M2	Sitges Beach, Spain	littoral	38.4±4.9		0.81±0.20
SH12-5A	Cueva Mayor exterior, Atapuerca, Spain	slopewash / aeolian	6.1±2.0		**0.25±0.15**
ATD14-MA1	Gran Dolina exterior, Atapuerca, Spain	slopewash / aeolian	6.6±2.8	**0.94±0.81**	**0.04±0.04**
ATG14-MA1	Galería exterior, Atapuerca, Spain	slopewash / aeolian	15.7±7.7		26.7±3.2
ELC16-MA1	Emu Leap Cave, Nullarbor Plains, Australia	slopewash / aeolian	**0.28±0.30**	**0.30±0.69**	**-0.03±0.04**
LB14-MA1	Leana's Breath Cave, Nullarbor Plains, Australia	slopewash / aeolian	20.5±4.9	31.0±8.3	14.6±3.2
BG16-MA1	Bone Gulch, Murray River, Australia	Slopewash / aeolian	3.7±1.0		**0.04±0.06**
AR10-MA	Arganda, Spain	fluvial	33.1±7.0	30.0±5.6	**0.51±0.40**
LC14-MA1	Lake Callabonna, Australia	fluvial	14.7±4.0		**0.25±0.27**
FR15-MA	Hookina Creek, Australia	fluvial	27.1±8.9		**1.5±1.2**
FC16-MA1	Fishermans Cliff, Murray River, Australia	fluvial	62.6±10.0		**-0.01±0.04**

Table S5 (a) Single-grain and (b) synthetic aliquot (100-grain aliquot) TT-OSL, TT-OSL$_{290}$ and OSL D_e summary statistics for the modern analogue samples. CAM$_{UL}$ D_e values that are consistent with 0 Gy at 2σ are shown in bold.

Reference	Site	Sample	Type of deposit	SG OSL		SG TT-OSL and $TT\text{-}OSL_{290}$	
				CAM_{UL} D_e (Gy)	Overdis-persion (Gy)	CAM_{UL} D_e (Gy)	Overdis-persion (Gy)
This study	Lake Eyre Williams Point, Australia	LE14-MA1	lacustrine	-0.02±0.02	0.10±0.02		
	Fairy Meadow Beach, Australia	FM12-1	littoral	0.02±0.01	0.08±0.01	1.7±0.9	2.8±0.9
	Cueva Mayor exterior, Atapuerca, Spain	SH12-5A	slopewash / aeolian			2.3±1.3	3.5±1.4
	Gran Dolina exterior, Atapuerca, Spain	ATD14-MA1	slopewash / aeolian	-0.03±0.04	0.10±0.04	0.02±0.11	0±0
	Galería exterior, Atapuerca, Spain	ATG14-MA1	slopewash / aeolian	0.04±0.03	0.06±0.03	1.6±0.9	3.7±0.8
	Emu Leap Cave, Nullarbor Plains, Australia	ELC16-MA1	slopewash / aeolian	-0.04±0.02	0.24±0.02	-0.06±0.12	0.25±0.18
		ELC16-MA1	slopewash / aeolian			0.07±0.49	2.2±0.5*
	Bone Gulch, Murray River, Australia	BG16-MA1	Slopewash / aeolian	-0.01±0.02	0.16±0.01		
	Arganda, Spain	AR10-MA	fluvial	0.20±0.10	0.71±0.09	0.02±0.18	0.18±0.37
		AR10-MA	fluvial			-0.11±0.50	0±0*
	Lake Callabonna, Australia	LC14-MA1	fluvial	-0.01±0.03	0.21±0.03	0.05±0.10	0.11±0.08
	Hookina Creek, Australia	FR15-MA	fluvial	0.02±0.01	0.04±0.01		
	Fishermans Cliff, Murray River, Australia	FC16-MA1	fluvial	0.02±0.01	0.09±0.01		
Gliganic et al., 2017	Cooper Creek, Australia	CC2	fluvial	0.03±0.03	0.03±0.01		
	Cooper Creek, Australia	CC3	fluvial	-0.03±0.05	0±0		
	Wollombi Brook, Australia	WB2	fluvial	-0.04±0.03	0±0		
	Wollombi Brook, Australia	WB5	fluvial	0.01±0.03	0.01±0.01		
	Wollombi Brook, Australia	WB7	fluvial	-0.03±0.02	0.02±0.01		
			Mean		**0.12**		**1.41**
			Median		**0.08**		**0.25**
			Standard error		**0.05**		**0.53**

Table S6 Published single-grain OSL and TT-OSL overdispersion values for well-bleached modern samples with weighted mean D_e values of 0 Gy at 2σ. These overdispersion values have all been calculated using the unlogged central age model (CAM_{UL}) of Arnold et al. (2009) and are expressed in Gy. TT-OSL overdispersion values derived using the $TT\text{-}OSL_{290}$ protocol are denoted with an asterisk.

Reference	Site	Sample	Type of deposit	SG TT-OSL and TT-OSL290 CAM D_e (Gy)	Overdis-persion (%)
Arnold et al., 2014	Sima de los Huesos, Atapuerca, Spain	SH12-1A	Allochthonous cave infill	701±31	19±5
		SH12-2A	Allochthonous cave infill	728±27	21±4
		SH12-3A	Allochthonous cave infill	713±42	42±5
		SH12-4A	Allochthonous cave infill	767±41	22±5
Demuro et al., 2014	Galería, Atapuerca, Spain	ATG10-1	Allochthonous cave infill	511±25	22±5
		ATG10-3	Allochthonous cave infill	572±29	23±5
		AT10-2	Allochthonous cave infill	591±37	32±6
		ATG10-7	Allochthonous cave infill	601±27	31±4
		ATG10-8	Allochthonous cave infill	546±21	20±4
		ATG10-9	Allochthonous cave infill	925±71	12±11
		ATG10-10	Allochthonous cave infill	813±90	24±11
		ATZ10-4	Allochthonous cave infill	937±66	19±8
		ATG10-4	Allochthonous cave infill	957±62	12±9
Arnold and Demuro, 2015	Gran Dolina, Atapuerca, Spain	F13	Allochthonous cave infill	778±38	0±0*
Arnold et al., 2015	Sima del Elefante, Atapuerca, Spain	ATE10-11	Allochthonous cave infill	519±17	25±3
Ollé et al., 2016	La Cansaladeta, Tarragona, Spain	BO13-10	Fluvial	618±36	22±7
		BO13-8	Fluvial	580±30	20±6
		BO13-9	Fluvial	588±26	19±5
Hamm et al., 2016	Warratyi Rock Shelter, Flinders Ranges, Australia	ERS-7	Slopewash / aeolian	168±12	24±8
Fu et al., 2017	Lake Eyre Williams Point, Australia	LE14-1	lacustrine	194±12	34±6
This study	Kelly Hill Cave, Kangaroo Island, Australia	KI14-12	Allochthonous cave infill	35.8±1.4	19±4
Demuro et al., submitted	Galería de las Estatuas, Atapuerca, Spain	GE16-7	Allochthonous cave infill	161±10	21±8
Bartz et al., submitted	Lower Moulouya River, Morocco	C-L3824	Fluvial	871±72	0±0
			Mean		**21.0**
			Median		**21.0**
			Standard error		**2.1**

Table S7 Published single-grain TT-OSL overdispersion values for geological (non-modern) samples that are reported to have been fully bleached at the time of deposition and have not been affected by post-depositional mixing. These overdispersion values have all been calculated using the central age model (CAM) of Galbraith et al. (1999). TT-OSL overdispersion values derived using the TT-OSL_{290} protocol are denoted with an asterisk.